Applied Catalysis B: Environmental 305 (2022) 121024

Contents lists available at ScienceDirect

Applied Catalysis B: Environmental

journal homepage: www.elsevier.com/locate/apcatb

Coupling nitrogen/oxygen self-doped biomass porous carbon cathode catalyst with $CuFeO_2$/biochar particle catalyst for the heterogeneous visible-light driven photo-electro-Fenton degradation of tetracycline

Shuaishuai Xin [a,b,c], Siyue Huo [a], Chunlei Zhang [a], Xiaoming Ma [a], Wenjie Liu [a], Yanjun Xin [b], Mengchun Gao [a,c,*]

[a] Key Lab of Marine Environment and Ecology, Ministry of Education, Ocean University of China, Qingdao 266100, China
[b] Qingdao Engineering Research Center for Rural Environment, College of Resources and Environment, Qingdao Agricultural University, Qingdao 266109, China
[c] Shandong Provincial Key Laboratory of Marine Environment and Geological Engineering, Ocean University of China, Qingdao 266100, China

ARTICLE INFO

Keywords:
Heterogeneous visible-light driven photo-electro-Fenton
$CuFeO_2$/biochar particle catalyst
H_2O_2 electrogeneration
Tetracycline
Toxicity analysis

ABSTRACT

The heterogeneous visible-light driven photo-electro-Fenton (H-VL-PEF) system was built to degrade tetracycline using nitrogen/oxygen biomass self-doped porous carbon (NO/PC) cathode catalyst coupling $CuFeO_2$/biochar particle catalyst. The NO/PC possessed the H_2O_2 selectivity of 85.3%, and the gas diffusion electrode with NO/PC as cathode catalyst (NO/PC-GDE) exhibited fine H_2O_2 electrogeneration performance and stability. The generated electrons on $CuFeO_2$/biochar by electrostatic induction and light excitation promoted $\equiv Fe^{3+}/\equiv Fe^{2+}$ and $\equiv Cu^{2+}/\equiv Cu^{+}$ redox cycle, which was beneficial for $HO^{\bullet}/O_2^{\bullet-}$ formation and tetracycline degradation. The introduction of $CuFeO_2$/biochar catalyst and visible light could reduce energy consumption and promote tetracycline mineralization. The $CuFeO_2$/biochar loads, initial pH and current density of H-VL-PEF system were optimized. The degradation pathway of tetracycline was speculated based on the intermediates identified by HPLC/MS. *Escherichia coli* growth inhibition experiments and toxicity prediction analysis demonstrated that the comprehensive toxicity of tetracycline was alleviated due to the catalytic degradation of H-VL-PEF system.

1. Introduction

Tetracycline, a popular broad-spectrum antimicrobial agent, has been extensively used in therapeutic medicine and livestock husbandry, causing a large amount of wastewater containing tetracycline to enter water environment. The residual tetracycline can induce the emergence antibiotic resistant bacteria and genes in ecological system [1]. Due to its stable molecular structure of aromatic rings, tetracycline is difficult to be degraded in natural condition [2]. The physical adsorption without mineralization can only separate tetracycline from water and faces the difficulty of adsorbent post-treatment [3]. The removal efficiency of tetracycline by biological degradation is very low due to its antibacterial nature [4]. Traditional chemical oxidation methods (e.g., chlorine oxidation and ozonation) have been applied to oxidize tetracycline, which have the shortcoming of producing carcinogenic chlorinated intermediates or high treatment costs [5,6]. Comparatively, electrochemical advanced oxidation processes (EAOPs) have received great attention for efficient degradation of tetracycline to smaller or inorganic substrates through producing high active hydroxyl radical ($^{\bullet}OH$) [7]. Anodic oxidation and electro-Fenton (EF) are two kinds of commonly popularized EAOPs. Anodic oxidation is based on the production of heterogeneous $^{\bullet}OH$ through water oxidation at metallic or metal oxide anode surface, whereas $^{\bullet}OH$ can be produced homogeneously in the solution during the EF process [8]. Notably, the electrogeneration of H_2O_2 can be achieved by two-electron oxygen reduction reaction (ORR) at an appropriate cathode during the EF process, which avoid the potential explosion risk of shipment, storage and handling of concentrated H_2O_2 [9,10]. The gas diffusion electrode (GDE) fabricated by cathode catalysts combined with polytetrafluoroethylene (PTFE) is regarded as the most effective cathode for H_2O_2 generation [11]. Precious metals and transition-metal based composites have been demonstrated as prospective cathode catalyst for H_2O_2 generation, whereas the high cost, scarcity and toxicity restricts their large-scale applications in EF process [12–14]. Therefore, it is necessary to develop efficient, green and economical cathode catalyst for tetracycline degradation in EF process.

Heteroatoms doped carbon materials, especially nitrogen and/or

* Corresponding author at: Key Lab of Marine Environment and Ecology, Ministry of Education, Ocean University of China, Qingdao 266100, China.
E-mail address: mengchungao@outlook.com (M. Gao).

https://doi.org/10.1016/j.apcatb.2021.121024
Received 10 September 2021; Received in revised form 12 December 2021; Accepted 17 December 2021
Available online 20 December 2021

oxygen doped carbons, are currently considered as alternatives to replace metal-based cathode catalyst for H_2O_2 generation owing to their lower cost, abundant reserves and excellent stability. The preparation of nitrogen doped carbons involved multiple steps and extra nitrogen precursors (e.g., aniline, pyrrole and ammonia gas) [15], and the oxidation of concentrated acids or strong oxidants is the familiar method to prepare oxygen doped carbon electrocatalysts for H_2O_2 generation [16]. However, the extra employment of nitrogen precursors, concentrated acids or strong oxidants adds both complexity and expense of material preparation. The transformation of biomass into heteroatom self-doped porous carbons for the ORR has attracted wide attentions owing to its abundant oxygen and nitrogen, such as chitosan [17], cornstalk [18], microalgae [19] and bamboo [20]. However, most previous studies focus on four-electron ORR using biomass-derived heteroatom self-doped carbons as catalyst to boost the reaction rate of the cathode in fuel cells. Alfalfa with high content of protein is one of the most widely planted crops all over the world and considered as an ideal precursor to prepare nitrogen or oxygen self-doped porous carbons [21]. The alfalfa-derived heteroatom self-doped carbons showed fine electrochemical performance in N_2 electroreduction reaction to ammonia and symmetrical supercapacitors [22,23]. Until now, it is still unclear whether the alfalfa-derived nitrogen and oxygen self-doped porous carbon (NO/PC) can be used as an effective cathode catalyst for H_2O_2 generation in EF process.

As is well known, the degradation efficiency of organic pollutant through the homogeneous EF process is unsatisfactory due to high energy consumption and low Fe^{2+} regeneration efficiency [24]. The EF performance can be significantly improved by constructing photo-electro-Fenton (PEF) process, which can be attributed to a higher reactive oxygen species production and the accelerated reduction of Fe^{3+} to Fe^{2+} through a series of photochemical reactions [25]. However, the homogeneous PEF process has some drawbacks during the degradation of organic pollutants, including strict pH reaction condition, higher iron sludge treatment cost and difficult recovery of Fe^{2+} [26]. Recently, numerous solid catalysts have attracted special attention in heterogeneous reaction process to replace soluble Fe^{2+}, such as monometallic iron oxides [27–29], transition metal particles [30], chalcopyrite [31] and polyvalent manganese [32]. However, the poor chemical stability and low visible light utilization of these heterogeneous catalysts limit their application in the heterogeneous PEF (H-PEF) process. To improve the performance of EF process and utilize the greater proportion of solar spectrum, it is necessary to develop a stable and effective heterogeneous visible-light (accounts for 43% of the total solar energy) driven photo-electro-Fenton (H-VL-PEF) particle catalyst to degrade pollutant from water. Previous study has verified that the $CuFeO_2$/-biochar prepared using hydrothermal method without reductant possessed high chemical stability, and the synergistic effects of Fe^{3+}/Fe^{2+} and Cu^{2+}/Cu^{+} redox cycle made $CuFeO_2$/biochar show high catalytic performance for H_2O_2 activation [33]. Simultaneously, the introduction of biochar can significantly improve the visible light photocatalytic performance of $CuFeO_2$ by relieving the recombination of the photoexcited carriers [34]. Hence, $CuFeO_2$/biochar might be potential and suitable particle catalyst in H-VL-PEF system. To our knowledge, there is no report regarding alfalfa-derived NO/PC cathode catalyst coupling $CuFeO_2$/biochar particle catalyst in H-VL-PEF system for tetracycline degradation.

The object of the present research was to assess the potential of H-VL-PEF system using GDE cathode with NO/PC catalyst (NO/PC-GDE) and $CuFeO_2$/biochar particle catalyst for tetracycline degradation. $CuFeO_2$/biochar was synthesized by hydrothermal method without extra reductant. NO/PC was prepared with alfalfa as a carbon precursor without chemical reagents (e.g., nitrogen sources, strong oxidants or concentrated acids) by pyrolysis method. The characterizations of $CuFeO_2$/biochar, NO/PC and NO/PC-GDE were systematically investigated by various analytical methods. The critical parameters influencing tetracycline degradation, including $CuFeO_2$/biochar loads, current density, initial pH and inorganic anions, were investigated in H-VL-PEF system. The recycling experiment for ten runs was performed to estimate the stability of H-VL-PEF system for tetracycline degradation. The reactive species, proposed mechanism and intermediates were clarified by a series of advanced technical methods. *Escherichia coli* growth inhibition experiments and Toxicity Estimation Software Tool (T.E.S.T.) software based on quantitative structure-activity relationship (QSAR) prediction were employed in assessing the comprehensive toxicity of tetracycline degraded by H-VL-PEF system.

2. Experimental

2.1. Synthesis of $CuFeO_2$/biochar and NO/PC catalyst

All chemicals were purchased from commercial sources and used without further purification for all experiments. The detailed information of all chemicals was provided in the Text S1. The $CuFeO_2$/biochar was synthesized by hydrothermal method without extra reductant in our previous investigation [33] and the detailed procedure was summarized in Text S2. The NO/PC catalyst was synthesized using alfalfa as carbon precursors at no extra nitrogen sources, strong oxidants or concentrated acids. Briefly, the mixture of alfalfa powder, potassium oxalate monohydrate and calcium carbonate with equal weight was fully ground in an agate mortar. The ground mixture was pyrolyzed at 500 °C with N_2 protection for 2 h with 5 °C min^{-1} of temperature-programmed rate. The pyrolytic powder was washed with diluted hydrochloric acid for several times to remove inorganic impurities. The black powder was gained through filtration and washed by deionized water, and dried overnight at 80 °C to obtain NO/PC catalyst.

2.2. Fabrication of GDE with NO/PC as cathode catalyst

In the fabrication of each GDE, a mixture of 0.15 g NO/PC as cathode catalyst, appropriate amount of ethanol and polytetrafluoroetylene (PTFE, 60%) emulsion as binder with typical mass NO/PC(g): PTFE (mL) ratio of 1:3 was dispersed through 10 min ultrasound. The nickel foam was selected as electrode substrate due to its superior conductivity, large surface area, good mechanical properties, small ventilation resistance and strong filling ability [35,36]. The dispersed mixture was turned into a gel by stirring at 80 °C and fully placed onto nickel foam surface in the form of gel/nickel foam/gel (1 × 3 cm, 1.0 mm thickness), and the Ni foam surface was completely covered by the mixture of NO/PC and PTFE emulsion. To acquire NO/PC-GDE, the above-mentioned gel/-nickel foam/gel was calcined at 350 °C for 60 min, then immersed into PTFE emulsion (30%) for 15 min and calcined at 300 °C for 60 min for enhancing the stability of NO/PC-GDE [37].

2.3. Characterization and electrochemical measurement

The X-ray powder diffraction (XRD) spectrum of $CuFeO_2$/biochar was recorded on a D8 Advance diffractometer (Bruker, Germany) with Cu kα radiation (λ = 1.5418 Å). The surface morphologies of $CuFeO_2$/biochar, NO/PC and NO/PC-GDE were investigated by scanning electron microscope (SEM, JEOL 7500 F). The X-ray photoelectron spectroscopy (XPS) and valence band XPS were determined with an ESCALAB 250XI spectrometer (Thermo). UV-Vis diffuse reflectance spectrum (DRS) of $CuFeO_2$/biochar was obtained from a UV–vis spectrophotometer (PUXI TU-1901) at wavelength of 300–800 nm with $BaSO_4$ as reference by pressing the $CuFeO_2$/biochar powder into disks directly. Photoluminescence (PL) spectra of $CuFeO_2$/biochar with and without light were obtained with a fluorescence spectrometer (Hitachi F-4600). The contact angles between NO/PC-GDE and water were measured on a goniometer (CA100A, China). The electrochemical properties of samples were measured using an electrochemical workstation (PGSTAT302N, Metrohm) with a graphite rob as counter electrode and Ag/AgCl as reference electrode. For the electrochemical

analysis of NO/PC or $CuFeO_2$/biochar, the working electrode was glassy carbon electrode loaded with NO/PCs or $CuFeO_2$/biochar (see Text S3 for load details). Electrochemical impedance spectroscopy (EIS) of $CuFeO_2$/biochar with and without light was performed with frequency range from 0.1 Hz to 100 kHz, and the photocurrent intensity was measured with the lamp on and off. The cyclic voltammetry (CV) curves of NO/PC were recorded in N_2 and O_2-saturated static solution at a scan rate of 100 mV s^{-1}, respectively. Linear sweep voltammetry (LSV) of NO/PC by rotating ring disk electrode (RRDE) was conducted at 5 mV s^{-1} and 1600 rpm with a Pt ring potential of 0.3 V (vs. Ag/AgCl). The calculated equations of electron transfer number, H_2O_2 selectivity and current efficiency were given in Text S3. In addition, the NO/PC-GDE was selected as working electrode to measure its electroactive surface area by CV analysis in the potential range of 0.60–0.80 V vs. Ag/AgCl and different scan rates (20–100 mV s^{-1}), and the measured details were provided in Text 4.

2.4. Experimental procedure and analysis

The performance of H-VL-PEF process using the fabricated NO/PC-GDE (1 × 3 cm) as cathode, a Pt plate (1 × 4 cm) as anode and a given dosage of $CuFeO_2$/biochar as particle catalyst was estimated in an undivided cell containing 250 mL tetracycline solution (20 mg L^{-1}) and 50 mM Na_2SO_4 electrolyte under visible light. The degradation process was controlled by a direct-current power in constant current mode, and the solution was irradiated using a Xe lamp equipped with an optical filter ($\lambda > 420$ nm). The dilute H_2SO_4 or NaOH solution was used to adjust initial pH of solution. During the reaction, continuous air was bubbled into the electrolyte near the cathode to provide enough oxygen for H_2O_2 generation. Samples were regularly taken out and filtrated immediately by 0.45 μm filter films for analysis. The specific energy consumption (EC) per unit tetracycline mass (kW h g^{-1} of tetracycline) using following equation:

$$EC = \frac{UIt}{(C_0\text{-}C)V} \quad (1)$$

Where U, I, t, C_0, C and V are average cell voltage (V), applied current (A), reaction time (h), initial concentration of tetracycline (mg L^{-1}), residual concentration of tetracycline (mg L^{-1}) and solution volume (L), respectively.

H_2O_2 accumulation and the concentrations of residual tetracycline were measured using potassium titanium(IV) oxalate method at 400 nm and spectrophotometric method at 357 nm, respectively [34]. Total organic carbon (TOC) was determined on a TOC analyzer for evaluating the mineralization of tetracycline. The leaching concentrations of iron and copper ions were detected through an Optima 8000 inductively coupled plasma optical emission system. The electron spin resonance (ESR) spectra were obtained on Bruker EMX EPR spectrometer to detect radical species. The degradation intermediates of tetracycline were identified through HPLC/MS technique, and the details were described in Text S5. The antimicrobial activities of tetracycline solution and reaction samples were tested using *Escherichia coli* ATCC 25922. Optical density (absorbance at 600 nm) and the inhibition zone diameter were used as indicators of *Escherichia coli* growth. The specific step of *Escherichia coli* growth inhibition experiments was described in Text S6. The toxicities of tetracycline and its intermediates were assessed through T.E.S.T. software.

3. Results and discussion

3.1. Characterizations of $CuFeO_2$/biochar and NO/PC

The XRD spectra in Fig. S1 presented that the diffraction peaks of $CuFeO_2$/biochar were consistent with the typical $CuFeO_2$ phase (PDF#39–0246, space group: R-3 m), indicating that $CuFeO_2$/biochar containing pure-phase $CuFeO_2$ was prepared in the current work. The SEM image of $CuFeO_2$/biochar showed that the $CuFeO_2$ was mainly distributed on biochar surface (Fig. 1a), and it was beneficial to expose more active sites. The energy dispersive X–ray spectra (Fig. S2) and the elemental mapping (Fig. 1b1 - b4) of the inset in SEM image of $CuFeO_2$/biochar revealed that C, O, Fe, and Cu coexisted in $CuFeO_2$/biochar, and the weight ratio of the $CuFeO_2$ was approximately 39% in $CuFeO_2$/biochar. The atomic ratio of Cu to Fe was close to 1:1, which conformed to the stoichiometry of $CuFeO_2$. The TEM and HRTEM spectra of $CuFeO_2$/biochar showed that the lattice spacing of 0.286, 0.251, 0.224 and 0.167 nm matched with Bragg reflections from (006), (012), (104) and (018) planes of $CuFeO_2$, respectively (Fig. S3), which was consistent with the XRD spectrum. After the introduction of visible light, the photocurrent density of $CuFeO_2$/biochar increased significantly (Fig. S4a), while its interfacial electron transfer resistance reduced (Fig. S4b), which indicated that the $CuFeO_2$/biochar possessed fine separation of photogenerated carriers and more effective charge kinetics [38]. Meanwhile, the PL spectra of $CuFeO_2$/biochar showed the excitation peak at the excitation wavelength of 425 nm (Fig. S4c), whereas no excitation peak was observed without illumination, suggesting that the transfer and recombination of photogenerated carriers occurred in $CuFeO_2$/biochar with light [32]. The present results confirmed that $CuFeO_2$/biochar has potential photocatalytic properties under visible light.

The morphology of NO/PC catalyst from the SEM image displayed an obvious three-dimensional porous structure (Fig. 1c and d), which was favorable to improve electrocatalytic performance. The corresponding elemental mapping of Fig. 1d depicted the distributions of C, O and N on the surface of NO/PC in Fig. 1d1 - d3, which suggested that NO/PC was successfully prepared with alfalfa as carbon precursor through pyrolysis at no extra nitrogen precursors, concentrated acids or strong oxidants. The XRD spectra illustrated a diffraction peak of NO/PC catalyst at around 23.6° corresponding to (002) plane of graphitic carbon (Fig. S1), which was lower than (002) plane (26.6°) of standard graphite (JCPDS No. 196 26–1079). This phenomenon may be associated with N-rich feature of graphene layer, which can promote mass transfer in electrochemical reaction [39]. The full-scale XPS spectrum showed the existence of C, O, and N elements on NO/PC catalyst (Fig. 2a), which was in accord with the result of the elemental mapping analysis. The C 1s XPS spectrum of NO/PC was divided into three peaks attributed to C═C/C-C (284.5 eV), C-O-C/C═N/C-OH (286.1 eV) and C═O/N-C═O (288.6 eV), which were account for 67.8%, 18.5% and 13.7%, respectively (Fig. 2b). The highest proportion of C═C/C-C suggested that biochar prepared by pyrolysis under nitrogen atmosphere possessed high degree of aromatization [40]. In the O 1s XPS spectrum (Fig. 2c), three signals at 531.4, 532.8 and 533.9 eV were respectively assigned to C═O (28.1%), C-O-C (36.9%) and C-OH (35.0%), suggesting the presence of rich oxygen-containing functional group on the NO/PC. The deconvolution of N1s XPS spectrum was shown in Fig. 2d, where three signals at 398.8, 400.4, and 401.1 eV were attributed to the pyridinic-N (29.4%), pyrrolic-N (35.0%), and graphitic-N (35.6%), respectively. The abundant C-O-C, pyrrolic-N and graphitic-N in the NO/PC can act as active sites for H_2O_2 electrogeneration via two-electron ORR process [16,39,41]. The CV and LSV have been carried out to further assess the ORR performance of NO/PC. As shown in Fig. 3a, no redox peak appeared in N_2-saturated medium, whereas a well-defined reduction peak was obtained with the potentials from − 0.2 to − 0.4 V vs. Ag/AgCl in O_2-saturated medium due to the two-electron ORR [42]. To further assess the selectivity toward two-electron ORR for H_2O_2 generation, the disk current (I_D) and ring current (I_R) were detected by RRDE in O_2-saturated solution at 5 mV s^{-1} and 1600 rpm with the fixed 0.3 V (vs. Ag/AgCl) at ring electrode to oxidize the generated H_2O_2 on disk electrode (Fig. 3b). The electron transfer number and the H_2O_2 selectivity of NO/PC were calculated based on Eqs. S1 and S2. Fig. S5 showed that the calculated electron transfer number of NO/PC was 2.3–2.5 with the potential from − 0.4 to − 1.0 V (vs. Ag/AgCl), indicating the

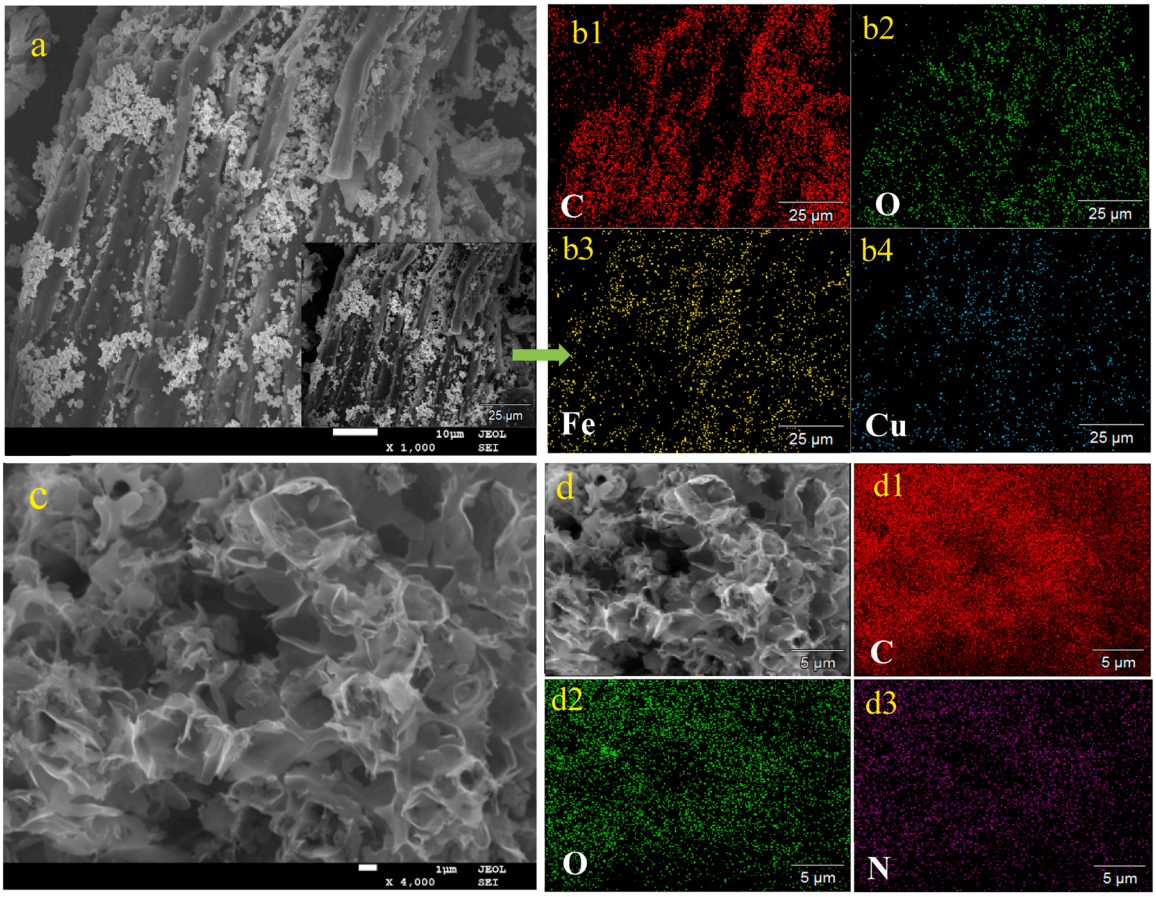

Fig. 1. SEM image of $CuFeO_2$/biochar (a) and elemental mapping images (b1- b4) corresponding to the inset in SEM image (a) of $CuFeO_2$/biochar, SEM images (c, d) of NO/PC and elemental mapping images (d1- d3) corresponding to the SEM image (d) of NO/PC.

dominance of two-electron ORR within the applied potential range. The highest H_2O_2 selectivity (85.3%) of NO/PC was acquired at − 0.423 V (vs. Ag/AgCl), which was higher than other reports of carbon catalysts, including N-doped graphene (58–76%) [42], chitosan-derived N-doped carbon (25%) [26], defective carbon-based materials (70%) [43], mesoporous non-metal N-doped carbon (~65%) [44], and COF-derived N-doped carbons (35–75%) [41]. Based on the above-mentioned results, the NO/PC was an effective carbon-based catalyst for H_2O_2 electrogeneration (Eq. 2).

$$O_2 + 2H^+ + e^- \rightarrow H_2O_2 \quad (2)$$

3.2. H_2O_2 accumulation and tetracycline degradation in various systems

As the organic pollutant degradation performance of EF in water treatment is closely associated with the electrogenerated yield of H_2O_2, the ability of fabricated NO/PC-GDE for generating H_2O_2 was explored at various systems without tetracycline. As depicted in Fig. 4a, the concentration of H_2O_2 accumulated to 13.4 ± 0.4 mM at current density of 80 mA cm^{-2} after 90 min in electrocatalysis system with NO/PC-GDE as cathode and Pt plate as anode. In general, superior hydrophobic cathode surface is conducive to the transfer of O_2 to active sites through a three-phase interface [45]. Besides, the low surface hydrophobicity of cathode will make electrolyte easier to diffuse to the cathode surface, which accelerated the occurrence of side reactions (Eqs. 3 and 4) at the cathode [26]. Thus, the proper hydrophobicity of cathode is beneficial to H_2O_2 electrogeneration.

$$2H_2O + 2e^- \rightarrow 2OH^- + H_2 \quad (3)$$

$$H_2O_2 + 2H^+ + 2e^- \rightarrow 2H_2O \quad (4)$$

The NO/PC-GDE surface was evenly covered with the PTFE layer, and almost no exposed NO/PC catalyst was observed (Fig. S6a), which led to good hydrophobicity with a water contact angle of 139.6° on the NO/PC-GDE surface (Fig. S6b). Furthermore, the electroactive surface area of NO/PC-GDE was evaluated by measuring the double-layer capacitance (Cdl) based on the CV curves at different scan rates (Fig. S7a). From the slopes as displayed in Fig. S7b, the Cdl value and electroactive surface area were calculated to be 10.05 mF and approximately 600 cm^2 for NO/PC-GDE, respectively [46]. These results indicated that NO/PC-GDE is an appropriate cathode to effectively generate H_2O_2 for its direct application in pollutants degradation from water by EF-based technologies. Notably, the accumulated concentration of H_2O_2 had some reduction in visible light+electrocatalysis system or H-EF ($CuFeO_2$/biochar+electrocatalysis) system (Fig. 4a), revealing that the introduction of visible light or $CuFeO_2$/biochar particle catalyst in electrocatalysis system could accelerate the decomposition of H_2O_2. The H_2O_2 concentration in H-VL-PFE system was 2.1 ± 0.3 mM after 90 min reaction, whereas the H_2O_2 concentration in electrocatalysis system was 13.4 ± 0.4 mM, which can be inferred that more active radicals were produced to degrade pollutants in H-VL-PFE system. When the tetracycline was added into the H-VL-PFE system, the H_2O_2 concentration further decreased to 1.7 ± 0.1 mM, which may be attributed to the direct molecular reaction between tetracycline and H_2O_2 [47].

Fig. 4b illustrated that the tetracycline degradation efficiency was less than 10% at pH 5.0 after 90 min of visible light irradiation, whereas 27.5 ± 0.8% of tetracycline was removed with $CuFeO_2$/biochar as catalyst in photocatalysis system. Additionally, the UV-Vis DRS spectrum of $CuFeO_2$/biochar showed a wide absorption under visible-light

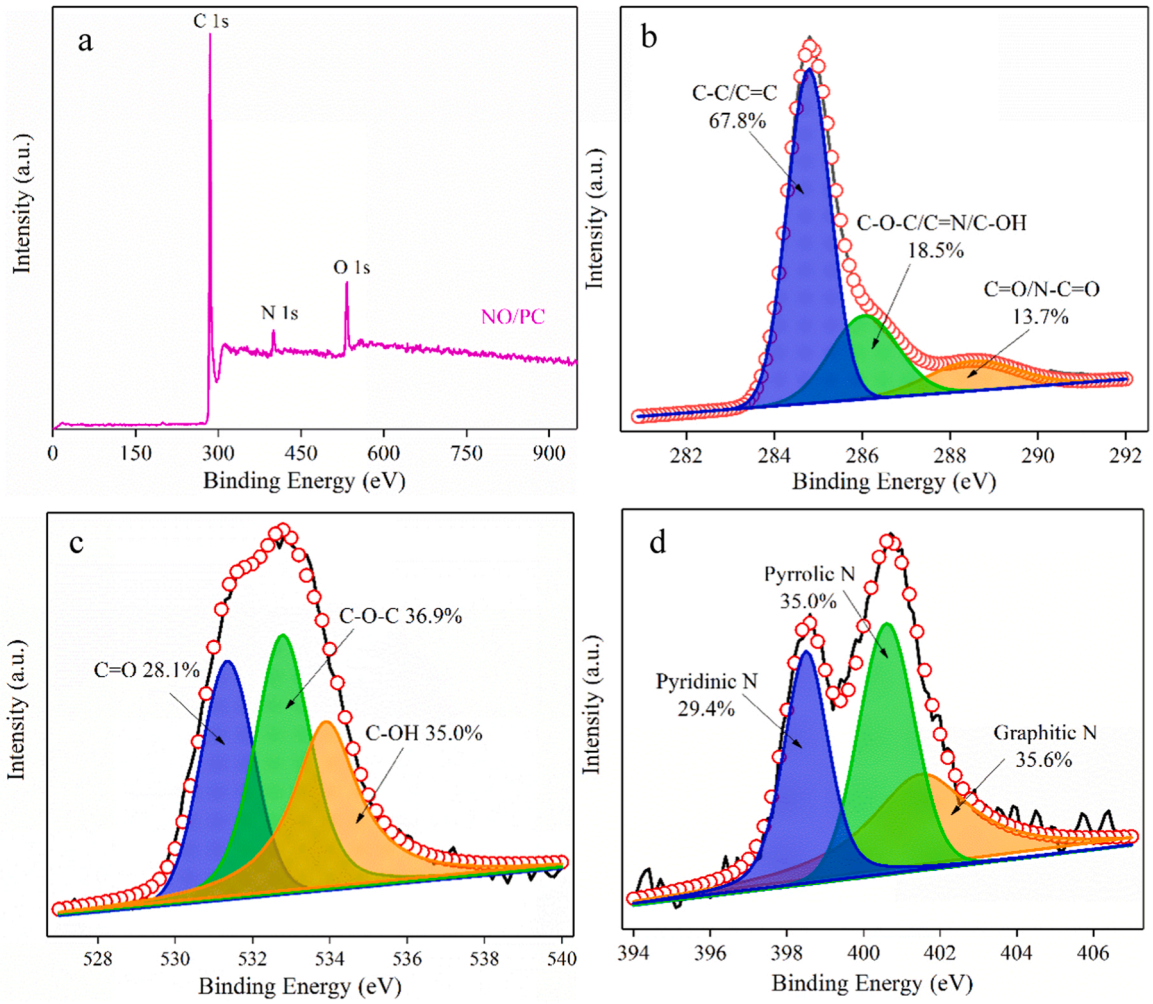

Fig. 2. XPS spectra of the overall survey (a), C 1s (b), O 1s (c) and N 1s (c) for NO/PC.

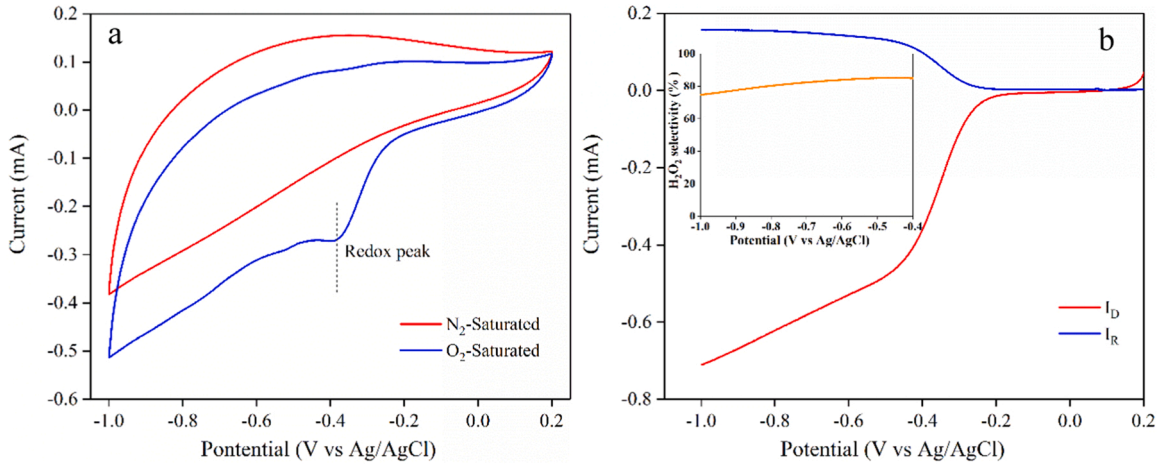

Fig. 3. CV curves (a) of NO/PC in O_2-saturated and N_2-saturated solution, ring current and disk current of RRDE measurement (b) and H_2O_2 selectivity (the inset) of NO/PC in O_2-saturated solution.

region, and the calculated band gaps energy of $CuFeO_2$/biochar was 2.40 eV according to *Kubelka-Munk* equation (Fig. S8a), which proved that $CuFeO_2$/biochar was an effective visible light photocatalyst. However, Fig. S8b illustrated that low valence band edge (1.54 eV) of $CuFeO_2$/biochar was observed in the XPS valence band spectrum, which resulted in lower tetracycline degradation efficiency using $CuFeO_2$/biochar as photocatalyst (Fig. 4b). Additionally, Fig. S9a showed that the sum of the tetracycline adsorption efficiency by $CuFeO_2$/biochar and NO/PC-GDE was less than 10% due to the low specific surface area (Fig. S10) of $CuFeO_2$/biochar and the good hydrophobicity (Fig. S6b) of NO/PC-GDE surface. For the electrocatalysis system, approximately 37.2 ± 0.7% tetracycline could be removed after 90 min, which was

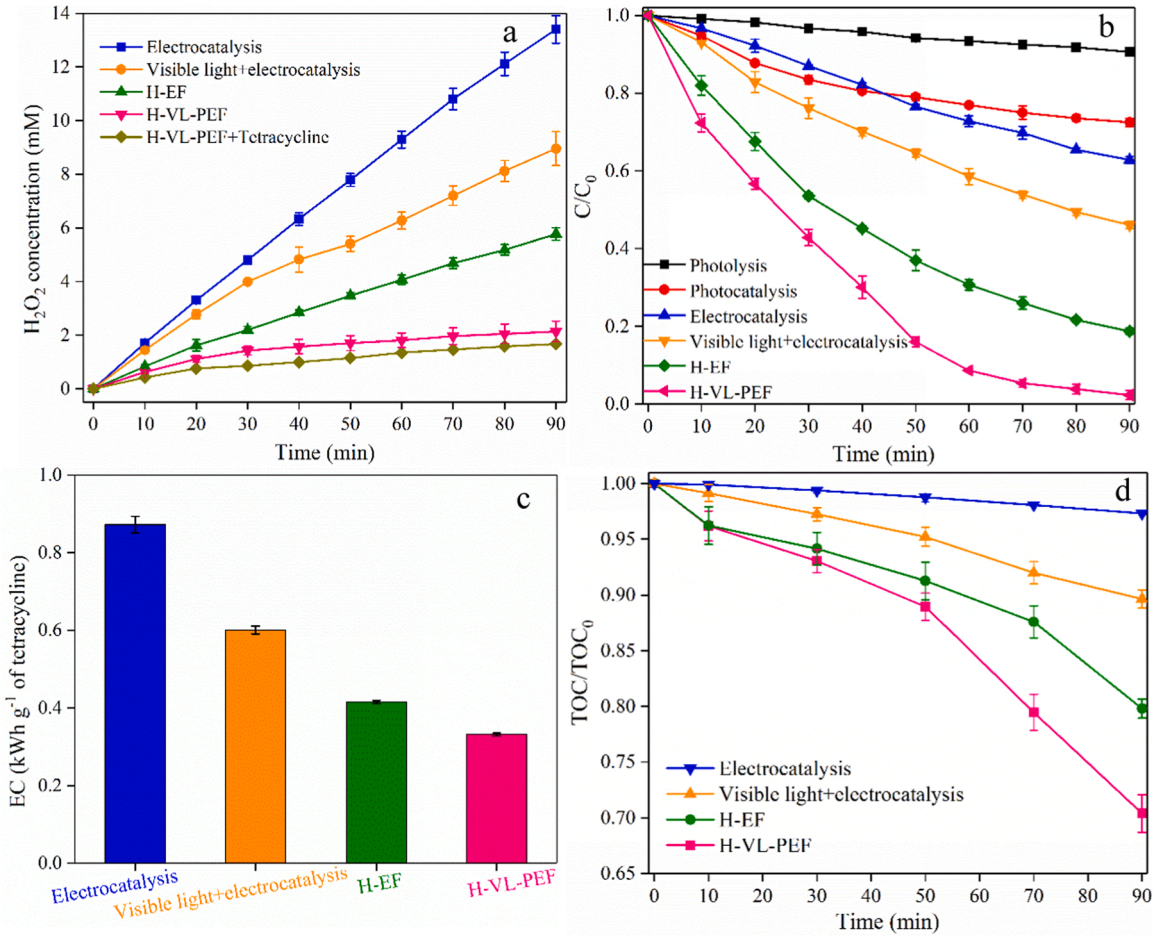

Fig. 4. H_2O_2 accumulation (a) and tetracycline degradation (b) in various systems. Energy consumption (c) and TOC removal (d) in electrocatalysis, visible light+electrocatalysis, H-EF and H-VL-PEF systems. ([$CuFeO_2$/biochar]$_0$ = 100 mg L^{-1}, [current density]$_0$ = 80 mA cm^{-2}, [tetracycline]$_0$ = 20 mg L^{-1} and pH = 5.0).

higher than total tetracycline degradation efficiency by 13.4 ± 0.4 mM H_2O_2 and anodic oxidation (Fig. S9b), which indicated that the NO/PC might transform generated H_2O_2 into active radicals. The tetracycline degradation efficiency increased to 81.2 ± 0.6% when $CuFeO_2$/biochar was added into electrocatalysis system, while the tetracycline degradation efficiency was only 23.3 ± 1.4% in $CuFeO_2$/biochar+ 13.4 mM H_2O_2 system (Fig. S9b), indicating that $CuFeO_2$/biochar could act as heterogeneous catalyst to activate generated H_2O_2 to produce more active radicals in H-EF system. Notably, the introduction of visible light significantly promoted tetracycline degradation in electrocatalysis and H-EF system. The highest tetracycline degradation efficiency was obtained at 97.7 ± 0.8% after 90 min in H-VL-PEF system. The energy consumptions after 90 min reaction for electrocatalysis, visible light+electrocatalysis, H-EF and H-VL-PEF were 0.872 ± 0.015, 0.601 ± 0.007, 0.416 ± 0.003, and 0.331 ± 0.003 kW h g^{-1} of tetracycline, respectively (Fig. 4c). Moreover, the removal efficiency (29.6 ± 1.2%) of TOC in H-VL-PEF system was higher than those in electrocatalysis system (2.7 ± 0.1%), visible light+electrocatalysis system (10.3 ± 0.7%) and H-EF system (20.2 ± 0.6%) after 90 min reaction (Fig. 4d). The present results clarity that the introduction of $CuFeO_2$/biochar catalyst and visible light can reduce energy consumption and promote tetracycline mineralization.

3.3. Influence of critical parameters on tetracycline degradation in H-VL-PEF system

3.3.1. Influence of $CuFeO_2$/biochar loads

The degradation efficiencies of tetracycline were evaluated under different $CuFeO_2$/biochar loads at current density of 80 mA cm^{-2} and pH 5.0 (Fig. 5a). The tetracycline degradation efficiency increased from approximately 65.3 ± 1.8% to 97.7 ± 0.8% after 90 min with $CuFeO_2$/biochar loads from 20 to 100 mg L^{-1}, suggesting that the increase of active sites and photogenerated carriers promoted active radical generation for tetracycline degradation in H-VL-PEF system [34]. Nevertheless, the degradation efficiencies of tetracycline were almost no variation with $CuFeO_2$/biochar from 100 to 150 mg L^{-1} and then decreased at 200 mg L^{-1} $CuFeO_2$/biochar. This phenomenon could be clarified that the increase of solution turbidity at higher $CuFeO_2$/biochar load was unfavorable for the penetration of light into solution [48].

3.3.2. Influence of current density

The current density can affect H_2O_2 generation by controlling the transfer of electrons between anode and cathode, which determines the production of active radicals in the EF-based technology [49]. To explore the influence of current density on the performance of H-VL-PEF system, the tetracycline degradation and H_2O_2 accumulation were investigated with current densities from 20 to 100 mA cm^{-2} in H-VL-PEF system and electrocatalysis system, respectively. As illustrated in Fig. 5b, the degradation efficiency of tetracycline increased from 58.2 ± 0.9% to 97.7 ± 0.8% after 90 min with current density

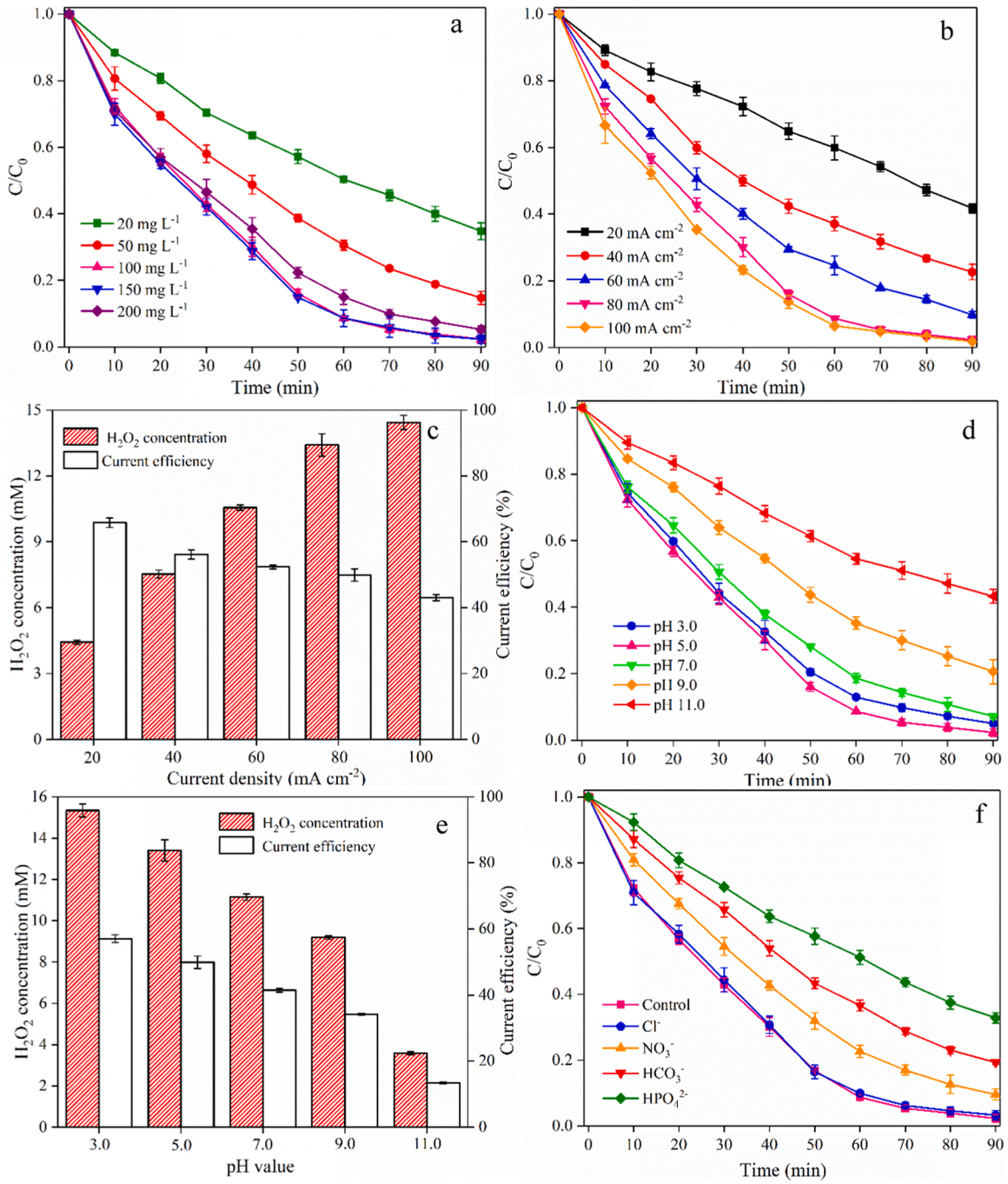

Fig. 5. Influence of $CuFeO_2$/biochar dosages (a), current densities (b), initial pH (d) and inorganic anions (f) on tetracycline degradation, and influence of current densities (c) and initial pH (e) on H_2O_2 electrogeneration. (Except for the investigated factors, the others were fixed on $[CuFeO_2/biochar]_0 = 100$ mg L^{-1}, [current density]$_0 = 80$ mA cm^{-2}, $[tetracycline]_0 = 20$ mg L^{-1} and pH = 5.0).

from 20 to 80 mA cm^{-2}, respectively. The accumulated concentration of H_2O_2 was promoted with the increase of current density in electrocatalysis system (Fig. 5c), which could lead to high tetracycline degradation efficiency at 80 mA cm^{-2}. However, the tetracycline degradation efficiency had no significant increase with the increase of current density from 80 to 100 mA cm^{-2} (Fig. 5b), which could be explained that more restricted mass transfer of O_2 towards cathode at higher current density caused the loss of oxidation efficiency in H-VL-PEF system [36]. Additionally, a higher current density would cause undesirable decomposition of H_2O_2 via side reactions (Eqs. 4–6) and limited H_2O_2 accumulation [50], which could cause an adverse effect on the tetracycline degradation and further decrease the current efficiency of H_2O_2 generation. For instance, the current efficiency decreased from 65.8 ± 1.0% to 43.0 ± 0.7% with current density from 20 to 100 mA cm^{-2} after 90 min in electrocatalysis system (Fig. 5c), which is consistent with the result of previous reports regarding H_2O_2 generation through two-electron ORR at cathode [37,45].

$$H_2O_2 \rightarrow H^+ + e^- + HO_2^{\bullet} \quad (5)$$

$$HO_2^{\bullet} \rightarrow O_2 + H^+ + e^- \quad (6)$$

3.3.3. *Influence of initial pH*

Fig. 5d illustrated that the tetracycline degradation efficiency decreased from 97.7 ± 0.8% at pH 5.0 to 92.8 ± 0.5% at pH 7.0,

79.4 ± 2.6% at pH 9.0, and 56.8 ± 1.5% at pH 11.0 at current density of 80 mA cm^{-2} after 90 min in H-VL-PEF system. The present results may be associated with the generation of H_2O_2 under different initial pH conditions. As shown in Fig. 5e, the accumulated concentration of H_2O_2 decreased from 13.4 ± 0.4 mM (current efficiency of 49.9 ± 1.4%) to 3.6 ± 0.1 mM (current efficiency of 13.3 ± 0.2%) with the initial pH from 5.0 to 11.0 in electrocatalysis system, suggesting that enough hydrogen ions under acidic conditions were available to generate H_2O_2 via Eq. (1). The deprotonation reaction of H_2O_2 (Eq. 7) was promoted by excess OH^- under neutral and alkaline conditions, which further destroy the accumulation of H_2O_2 in solution. Furthermore, the generation of $^{\bullet}OH$ can be accelerated through Eq. (8) employing $CuFeO_2$-based catalyst to activate H_2O_2 at lower pH value [51], which was beneficial to tetracycline degradation.

$$H_2O_2 \leftrightarrow H^+ + HO_2^- \quad (7)$$

$$Cu^+/Fe^{2+} + H_2O_2 + H^+ \rightarrow Cu^{2+}/Fe^{3+} + H_2O + HO^{\bullet} \quad (8)$$

Although the accumulated concentration of H_2O_2 increased to 15.3 ± 0.2 mM when the initial pH was further declined to pH 3.0, the tetracycline degradation of H-VL-PEF system was still inhibited. It is reported that excess hydrogen ions at pH 3.0 can convert H_2O_2 into a stable and electrophilic oxonium form via Eq. (9), whereas the reactivity is low for $HO^{\bullet}$ generation by the reaction between oxonium and catalyst [52]. The excess hydrogen ions have also an adverse effect on pollution degradation using Fenton-based technology through quenching $HO^{\bullet}$ (Eq. 10). Moreover, the tetracycline molecules exist predominantly as H_2TC^0 species at pH 5.0, which is more susceptible to active radical attack than H_3TC^+ formed at pH 3.0 owing to higher electron density in the ring of H_2TC^0 than H_3TC^+ [47].

$$H^+ + H_2O_2 \rightarrow H_3O_2^+ \quad (9)$$

$$H^+ + HO^{\bullet} + e^+ \rightarrow H_2O \quad (10)$$

3.3.4. Influence of inorganic anions

The practical water containing tetracycline generally exists dissolved inorganic anions (e.g., Cl^-, NO_3^-, HCO_3^- and PO_4^{3-}) which may interfere with the degradation process, thus the influence of inorganic anion on tetracycline degradation efficiency was investigated at the concentration of 10 mM (Fig. 5f). The addition of Cl^- had no significant inhibited influence on tetracycline degradation compared with the control group (No anions). Although Cl^- can react with $^{\bullet}OH$ to generate $ClOH^{\bullet-}$ with a rate constant of 4.3 ± 0.4 × 10^9 M^{-1} s^{-1} (Eq. 11), the dissociation of $ClOH^{\bullet-}$ can rapidly regenerate $HO^{\bullet}$ with higher rate constant (6.1 ± 0.8 × 10^9 M^{-1} s^{-1}) near neutral pH values (Eq. 12) [53]. However, tetracycline degradation decreased from 97.7 ± 0.8% to 90.4 ± 1.2% and 80.7 ± 0.4% when NO_3^- and HCO_3^- were added into H-VL-PEF system. It was reported that NO_3^- is inefficient for scavenging $HO^{\bullet}$ due to slow rate constant ($k < 5.0 \times 10^5$ M^{-1} s^{-1}) between $HO^{\bullet}$ and NO_3^- [54], whereas the complexation of NO_3^- with $CuFeO_2$/biochar might influence H_2O_2 activation and thus decrease tetracycline degradation efficiency [55]. The existence of HCO_3^- can form a CO_3^{2-}/HCO_3^- equilibrium system where HCO_3^- and CO_3^{2-} can transform $HO^{\bullet}$ to $CO_3^{\bullet-}$ with lower oxidation activity (Eqs. 13 and 14). Moreover, HPO_4^{2-} had greater inhibition on tetracycline degradation than other inorganic anions, which be attributed to the fact that HPO_4^{2-} not only serve as a scavenger to capture $HO^{\bullet}$ (Eq. 15), but also cause poisoning of the surface sites responsible for H_2O_2 activation by occupying surface active sites of $CuFeO_2$/biochar [56].

$$Cl^+ + HO^{\bullet} \rightarrow ClOH^{\bullet-} \quad (11)$$

$$ClOH^{\bullet-} \rightarrow Cl^+ + HO^{\bullet} \quad (12)$$

$$HCO_3^- + HO^{\bullet} \rightarrow CO_3^{\bullet-} + H_2O \quad (13)$$

$$CO_3^{2-} + HO^{\bullet} \rightarrow CO_3^{\bullet-} + OH^- \quad (14)$$

$$HPO_4^{2-} + HO^{\bullet} \rightarrow HPO_4^{\bullet-} + OH^- \quad (15)$$

3.4. Stability and reusability

To estimate the pollutant degradation performance of H-VL-PEF system under long-term operation, the NO/PC-GDE stability and $CuFeO_2$/biochar reusability were investigated by continuous H_2O_2 generation and tetracycline degradation cycle experiments at 80 mA cm^{-2} and pH 5.0 (Fig. 6). As shown in Fig. 6a, the H_2O_2 concentration and current efficiency have no obvious change during 10 continuous experiments in electrocatalysis system, indicating that NO/PC-GDE exhibits superior stability for H_2O_2 generation. It is reported that surface hydrophobicity of carbon-PTFE GDEs is a key factor affecting the H_2O_2 generation performance in long-term operation processes [37]. The contact angle between NO/PC-GDE and water only reduced from 139.6° to 131.0° after 10 cycles (900 min) due to the actions of electro-wetting (Fig. S11), which further proved the stability of NO/PC-GDE. Fig. 6b showed that the tetracycline degradation efficiency decreased by 12.3% after 10 cycles, suggesting that H-VL-PEF system had high stability for tetracycline degradation. The XRD spectrum of $CuFeO_2$/biochar illustrated no distinct variation of characteristic peaks before and after 10 cycles for tetracycline degradation (Fig. 6c). The surface survey XPS spectra demonstrated the existence of C, O, Fe and Cu in $CuFeO_2$/biochar before and after reaction, and these elemental peaks were nearly unchanged (Fig. 6d). Moreover, metal ion leaching might be another possible reason for the passivation of $CuFeO_2$/biochar, and the average leaching concentrations of total Fe and Cu ions in recycling experiments respectively were 0.020 ± 0.003 mg L^{-1} and 0.009 ± 0.003 mg L^{-1} (Fig. S12), which were much lower than the maximum discharge limited values of 15 mg L^{-1} Fe and 1.0 mg L^{-1} Cu from wastewater in rivers and lakes [57]. The above results have further demonstrated the stability of $CuFeO_2$/biochar in H-VL-PEF system for tetracycline degradation.

3.5. Identification of reactive species

To identify the contribution of reactive species to tetracycline degradation in H-VL-PEF system, excessive ammonium oxalate (AO), $AgNO_3$, methyl alcohol (MA) and benzoquinone (BQ) were selected to quench holes, electrons, $HO^{\bullet}$ and $O_2^{\bullet-}$, respectively. In general, photoinduced holes had promotional effects on pollution degradation in photocatalytic system, while AO had a slight promoting effect on tetracycline degradation compared with the control group without scavengers (Fig. 7a). This phenomenon might be explained that the addition of AO could inhibit the recombination of photoinduced carriers and result in more production of photoinduced electrons, which could accelerate Fe^{2+}/Fe^{3+} and Cu^+/Cu^{2+} cycles and was beneficial to the formation of reactive species for tetracycline degradation [58]. In addition, $CuFeO_2$/biochar could be polarized into a lot of microelectrodes due to electrostatic induction after the onset of power in H-VL-PEF system, which caused the accumulation of numerous electrons on $CuFeO_2$/biochar side close to the anode and further promoted Fe^{2+}/Fe^{3+} and Cu^+/Cu^{2+} cycles [11]. The presence of $AgNO_3$ as electrons scavenger had almost no influence on H_2O_2 generation in electrocatalysis system (Fig. S13), which may be attributed to that the good hydrophobicity on the NO/PC-GDE surface was detrimental to the diffusion of $AgNO_3$ in electrolyte into the internal pores of the NO/PC-GDE for electron trapping. Nevertheless, the tetracycline degradation efficiency declined from 97.7 ± 0.8% of the control group to 58.7 ± 0.9% when $AgNO_3$ was added into H-VL-PEF system (Fig. 7a), demonstrating that the electrons generated on $CuFeO_2$/biochar by electrostatic induction and light excitation play a key role in promoting tetracycline degradation. Furthermore, the tetracycline degradation

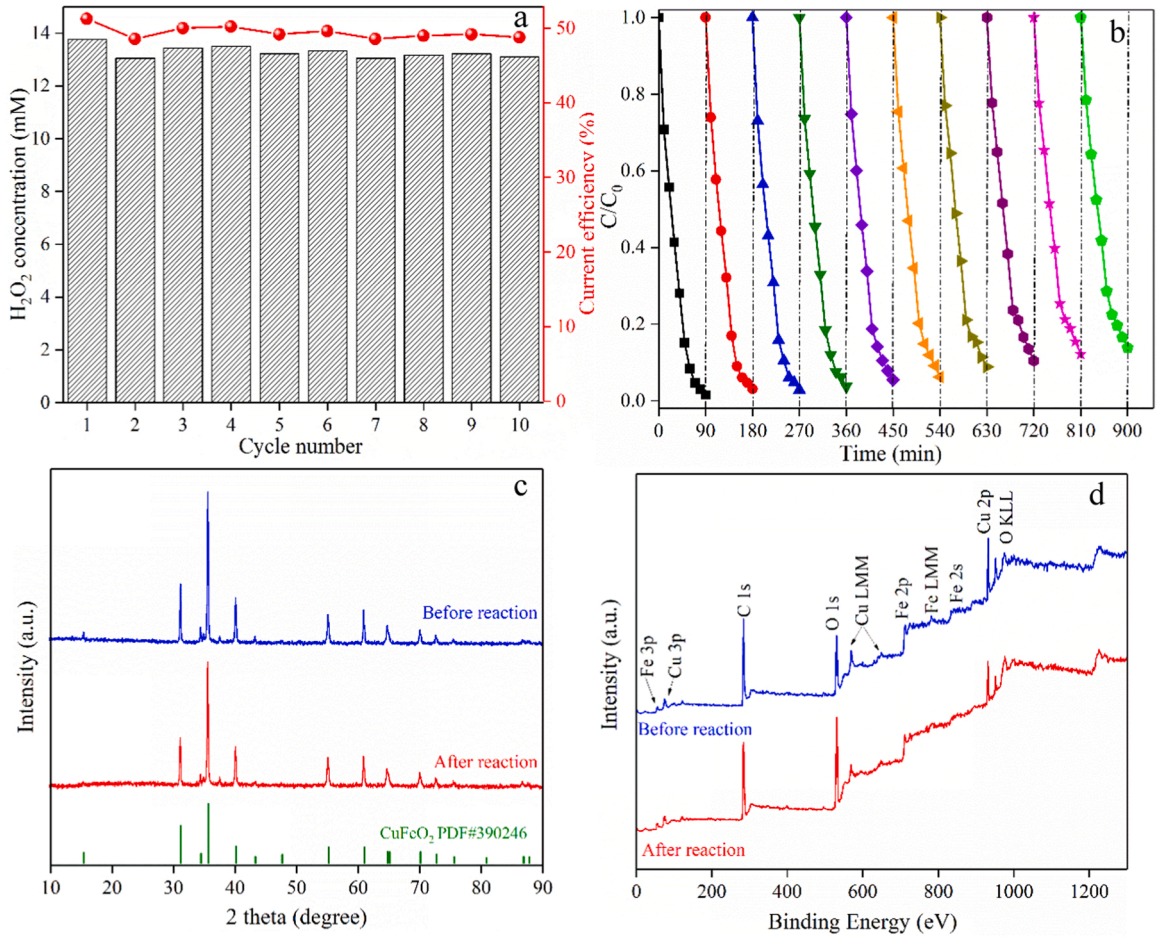

Fig. 6. The stability of NO/PC-GDE for H_2O_2 electrogeneration in electrocatalysis system (a), tetracycline cycle degradations (b) in H-VL-PEF system, XRD pattern (c) and surface survey XPS spectra (d) of $CuFeO_2$/biochar before and after reaction. ([$CuFeO_2$/biochar]$_0$ = 100 mg L^{-1}, [current density]$_0$ = 80 mA cm^{-2}, [tetracycline]$_0$ = 20 mg L^{-1} and pH = 5.0).

efficiency declined by 61.5 ± 1.2% as the addition of MA, whereas only 19.6 ± 0.4% inhibition appeared in the addition of BQ comparing to the absence of scavengers. The present results proved that $HO^•$ and electrons were the predominant reactive species, and $O_2^{•-}$ was subsidiary species for tetracycline degradation in H-VL-PEF system.

The ESR/DMPO experiment was further conducted to clarify the production of active radicals in different systems. As displayed in Fig. 7b and c, the weak signals of DMPO-$HO^•$ and DMPO-$O_2^{•-}$ were observed in electrocatalysis system, which could explain that the presence of pyridinic N in NO/PC activated generated H_2O_2 to produce active radicals [42]. The low tetracycline degradation efficiency in electrocatalysis system illustrated the low efficiency of NO/PC for H_2O_2 activation (Fig. 4b), resulting in high energy consumption and time costs. However, the intensity of DMPO-$HO^•$ and DMPO-$O_2^{•-}$ signals showed an obvious increase when visible light or $CuFeO_2$/biochar was introduced into electrocatalysis system, suggesting that visible light or $CuFeO_2$/-biochar could promote the H_2O_2 activation to produce active radicals and improve tetracycline degradation efficiency (Fig. 4b). Notably, DMPO-$HO^•$ and DMPO-$O_2^{•-}$ signals exhibited the highest intensity when both visible light and $CuFeO_2$/biochar were introduced in H-VL-PEF system than other degradation systems, which further demonstrated that H-VL-PEF system had good performance of producing active radicals to degrade tetracycline.

3.6. Proposed mechanism

In H-VL-PEF system, oxygen was supplied externally to the hydrophobic NO/PC-GDE surface and could effectively diffuse onto the active sites of NO/PC catalyst through a three-phase interface. Heteroatom doping on NO/PC catalyst could cause charge delocalization of nearby C atoms due to the higher electronegativity of O (3.44) and N (3.04) comparing with C (2.55) atom, which benefited the adsorption of oxygen on NO/PC surface and contributed to the reduction of oxygen to H_2O_2 by two-electron pathway [41,42]. Only a small portion of generated H_2O_2 was activated by NO/PC to form active radicals for tetracycline degradation, whereas most H_2O_2 diffused into the electrolyte and then reacted with $CuFeO_2$/biochar under visible light.

The Raman and XPS spectra of $CuFeO_2$/biochar before and after reaction were analyzed to further investigate the role of $CuFeO_2$/biochar for active radicals generation in H-VL-PEF system. Raman spectra (Fig. S14) of $CuFeO_2$/biochar before and after reaction displayed two sharp peaks at 1349 cm^{-1} (D band) and 1580 cm^{-1} (G band), which was identified as edge defects and graphitic carbon in $CuFeO_2$/biochar, respectively. The relative intensities of D and G bands (I_D/I_G) could be used to evaluate the degree of structurally ordered graphite crystallites in carbon materials [59]. The I_D/I_G value of $CuFeO_2$/biochar decreased from 0.99 to 0.93 after reaction possibly as the result of defective edge damage and surface functional groups variation, indicating that the defective sites of $CuFeO_2$/biochar took part in catalytic degradation of tetracycline [60]. The C 1 s XPS spectra illustrated that the C-C/C═C (284.8 eV) proportion of $CuFeO_2$/biochar decreased from 76.1% to 62.4% after reaction, while the percentage of C-OH/C-O-C (286.1 eV) and C═O (288.5 eV) increased from 14.3% to 22.5% and 9.6% to 15.1%, respectively (Fig. 8a), indicating that the C-C/C═C on

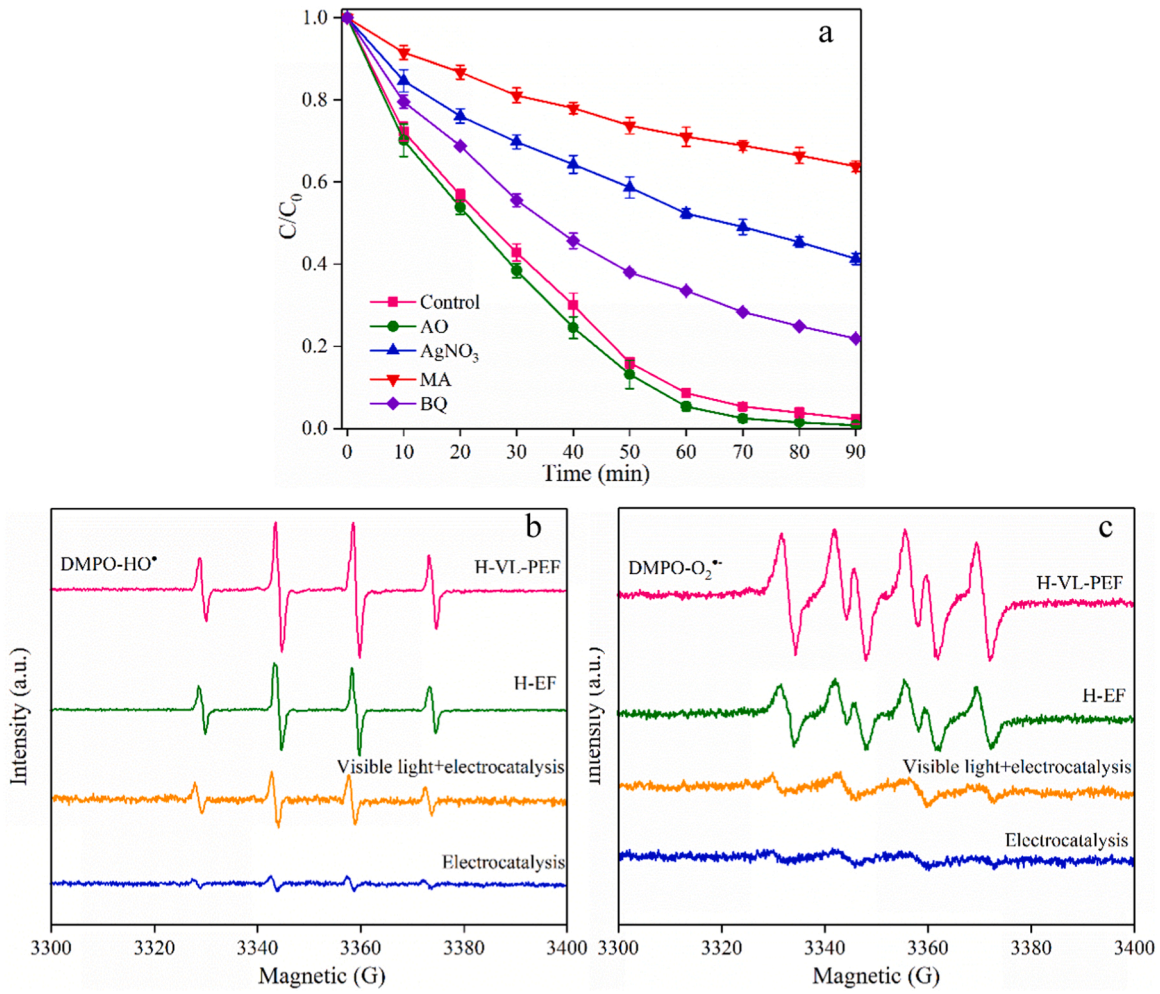

Fig. 7. Reactive species quenching experiments for tetracycline degradation in H-VL-PEF system (a), and ESR spectra of DMPO-$^{\bullet}$OH (b) and DMPO-$^{\bullet}O_2^-$ (c) in various systems. ([scavengers]$_0$ = 100 mM [$CuFeO_2$/biochar]$_0$ = 100 mg L^{-1}, [current density]$_0$ = 80 mA cm^{-2}, [tetracycline]$_0$ = 20 mg L^{-1} and pH = 5.0).

$CuFeO_2$/biochar surface could be partially oxidized to C-OH/C-O-C and C═O by active radicals [61]. The Fe 2p XPS spectra displayed that ≡Fe^{3+} species (≡ represents the element on solid catalyst surface) were located at 713.2 and 726.4 eV along with two satellite signals at 718.9 and 732.5 eV, while the peaks at 710.9 and 723.28 eV were assigned to ≡Fe^{2+} species (Fig. 8b). The peaks of Cu 2p XPS spectra at 932.6 and 952.4 eV were attributed to ≡Cu^{+} species, and the peaks at higher binding energies corresponded to ≡Cu^{2+} species (Fig. 8c). The ≡Fe^{3+}/≡Fe^{2+} ratio and ≡Cu^{2+}/≡Cu^{+} ratio in $CuFeO_2$/biochar was changed after reaction, suggesting that both Fe and Cu was involved in the H_2O_2 activation. In the O 1 s XPS spectra (Fig. 8d), the peaks centered at 529.9 eV, 531.5 eV and 533.26 eV corresponded to lattice oxygen (O_{lat}), surface hydroxyl group (-OH) and H_2O, respectively. The -OH and H_2O proportions of $CuFeO_2$/biochar before and after reaction increased from 42.7% to 47.4% and 21.2% to21.9%, respectively. The present results implied that ≡Cu^{+}/≡Cu^{2+} and ≡Fe^{3+}/≡Fe^{2+} species on $CuFeO_2$/biochar surface could act as Lewis sites and react with H_2O to generate the protonic acid sites (Eqs. 16 and 17), which contributed to the promotion of active radical production [51]. The formed ≡Cu^{+}-OH reacted with H_2O_2 to produce HO$^{\bullet}$ (Eq. 18), and then ≡Cu^{+}-OH was further reduced to ≡Cu^{+}-OH and $O_2^{\bullet-}$ by H_2O_2 through intramolecular electron transfer (Eq. 19). Additionally, the reduction of ≡Fe^{3+}-OH to ≡Fe^{2+}-OH by ≡Cu^{+}-OH could be realized via Eq. (20) due to higher redox potential (E^0 = 0.77 V vs NHE) of Fe^{3+}/Fe^{2+} than that (E^0 = 0.17 V vs NHE) of Cu^{2+}/Cu^{+} [33]. The ≡Fe^{2+}-OH also was generated from reduction of ≡Fe^{3+}-OH by H_2O_2 and O_{lat} (Eqs. 21 and 22), which led to the relative content of O_{lat} in $CuFeO_2$/biochar decreased from 32.2% to 29.7% after reaction (Fig. 8d). The generated ≡Fe^{2+}-OH could activate H_2O_2 in a mechanism like Haber-Weiss process to produce •OH (Eq. 23).

$$\equiv Cu^{+}/Cu^{2+} + H_2O \rightarrow \equiv Cu^{+}/Cu^{2+}\text{-}OH^{-} + H^{+} \quad (16)$$

$$\equiv Fe^{3+}/Fe^{2+} + H_2O \rightarrow \equiv Fe^{3+}/Fe^{2+}\text{-}OH^{-} + H^{+} \quad (17)$$

$$\equiv Cu^{+}\text{-}OH^{-} + H_2O_2 \rightarrow \equiv Cu^{2+}\text{-}OH^{-} + HO^{\bullet} + OH^{-} \quad (18)$$

$$\equiv Cu^{2+}\text{-}OH^{-} + H_2O_2 \rightarrow \equiv Cu^{+}\text{-}OH^{-} + O_2^{\bullet-} + 2H^{+} \quad (19)$$

$$\equiv Fe^{3+}\text{-}OH^{-} \equiv Cu^{+}\text{-}OH^{-} \rightarrow \equiv Fe^{2+}\text{-}OH^{-} \equiv Cu^{2+}\text{-}OH^{-} \quad (20)$$

$$\equiv Fe^{3+}\text{-}OH^{-} + H_2O_2 \rightarrow \equiv Fe^{2+}\text{-}OH^{-} + O_2^{\bullet-} + 2H^{+} \quad (21)$$

$$\equiv Fe^{3+}\text{-}OH^{-} + 2O_{lat} \rightarrow \equiv Fe^{2+}\text{-}OH^{-} + O_2 \quad (22)$$

$$\equiv {}^{2+}\text{-}OH^{-} + H_2O_2 \rightarrow \equiv Fe^{3+}\text{-}OH^{-} + HO^{\bullet} + OH^{-} \quad (23)$$

Although the associated effects of ≡Fe^{3+}-OH/≡Fe^{2+}-OH and ≡Cu^{2+}-OH/≡Cu^{+}-OH redox cycle promoted the catalytic activity of $CuFeO_2$/biochar for H_2O_2, the limited regeneration rate of ≡Cu^{+} and ≡Fe^{2+} by Eqs. (19)–(22) caused low tetracycline degradation efficiency in heterogeneous Fenton system (Fig. S9b) [33]. Notably, $CuFeO_2$/-biochar was polarized under the action of electric field in H-VL-PEF

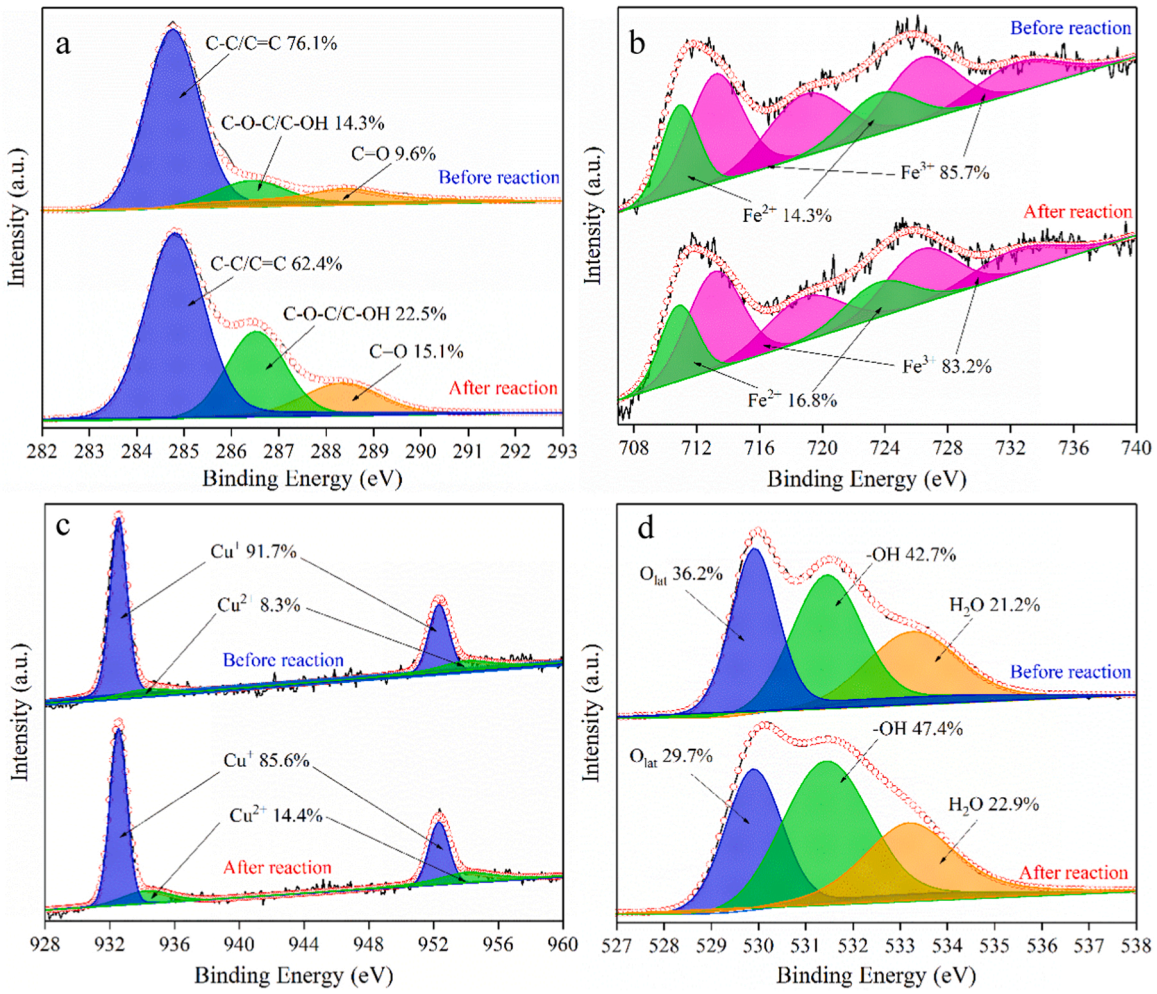

Fig. 8. The high-resolution XPS spectra of C 1s (a), Fe 2p (b), Cu 2p (c) and O 1s (d) for $CuFeO_2$/biochar catalyst before and after reaction.

system, and the electrons produced by polarization could accelerate the regeneration of $\equiv Cu^{2+}$-OH to $\equiv Cu^{+}$-OH and $\equiv Fe^{3+}$-OH to $\equiv Fe^{2+}$-OH through Eqs. (24) and (25). Meanwhile, $CuFeO_2$/biochar was excited by visible light radiation to produce photoinduced holes and electrons on its valence band and conduction band, respectively (Eq. 26). The holes cannot oxidize H_2O or OH^- to generate $HO^\bullet$ owing to lower valence band edge (1.54 eV) of $CuFeO_2$/biochar (Fig. S8b) than $HO^\bullet/H_2O$ (2.68 eV vs NHE) or $HO^\bullet/OH^-$ (1.99 eV vs NHE) [62]. However, the production of

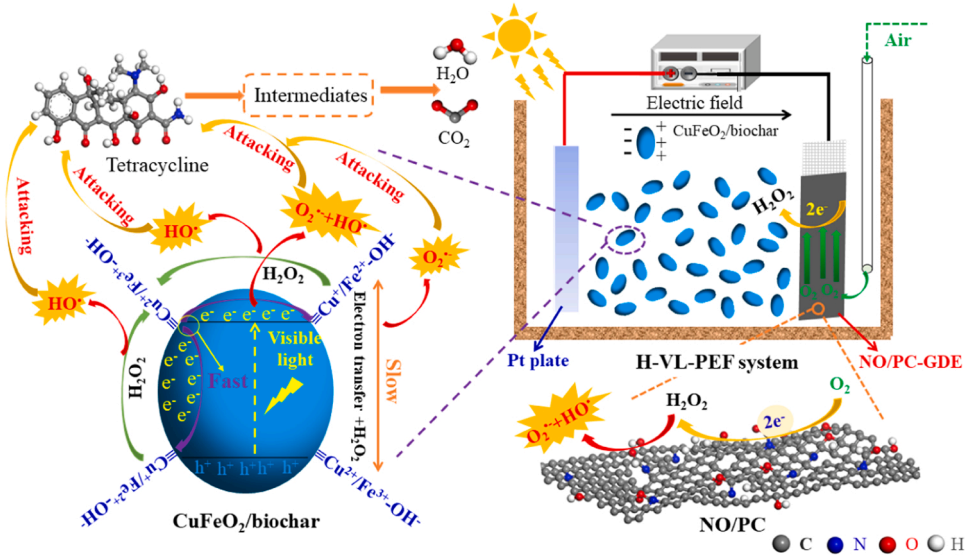

Fig. 9. Possible mechanism of tetracycline degradation in H-VL-PEF system.

photoinduced electrons could react with H_2O_2 and O_2 to produce $HO^•$ and $O_2^{•-}$ (Eqs. 27 and 28), but also further accelerated $\equiv Fe^{3+}$-OH/$\equiv Fe^{2+}$-OH and $\equiv Cu^{2+}$-OH/$\equiv Cu^{+}$-OH redox cycle by Eqs. (24) and (25), which was conducive to the production of active radicals. In addition, the $HO^•$ was also produced by direct photolysis of H_2O_2 (Eq. 29), and then the generated active radicals ($HO^•/O_2^{•-}$) degraded tetracycline into intermediates and final mineralized products (Eq. 30). The possible mechanism of tetracycline degradation in H-VL-PEF system was proposed in Fig. 9.

$$\equiv {}^{3+}\text{-OH} + e^- \rightarrow \equiv Fe^{2+}\text{-OH} \quad (24)$$

$$\equiv {}^{2+}\text{-OH} + e^- \rightarrow \equiv Cu^{+}\text{-OH} \quad (25)$$

$$\text{CuFeO2/biochar} + h\nu \rightarrow h^+ + e^- \quad (26)$$

$$e^- + H_2O_2 \rightarrow HO^• + OH^- \quad (27)$$

$$e^- + O_2 \rightarrow O_2^{•-} \quad (28)$$

$$h\nu + H_2O_2 \rightarrow 2HO^• \quad (29)$$

$$HO^•/O_2^{•-} + \text{Tetracycline} \rightarrow \text{Intermediates} \rightarrow CO_2 + H_2O \quad (30)$$

3.7. Degradation intermediates and toxicity estimation

To clarify the degradation pathway of tetracycline, the major intermediates were identified under HPLC/MS positive ion model. Based on the HPLC-MS spectra (Fig. S15), the degradation pathway of tetracycline was speculated in Fig. 10. The pathway I displayed that the tetracycline molecule ($m/z = 445$) was transformed to P1 ($m/z = 417$) by the detachment of two methyl groups at the tertiary amine [63], and then P2 ($m/z = 379$), P3 ($m/z = 265$) and P4 ($m/z = 239$) were generated via ring cleaving, double carbon bonds breaking and the abscission of amino and carbonyl groups. The formation of P5 ($m/z = 346$) was ascribed to the loss of H_2O molecule from P4, and the further intermediates P6 ($m/z = 182$) and P7 ($m/z = 125$) were caused by ring-opening reaction and losing methylene and carbonyl groups. The pathway II was regarded as multiple hydroxylation of tetracycline molecule under the attack of $HO^•$ to generated P8 ($m/z = 477$) [64]. Subsequently, the P9 ($m/z = 416$) was derived through the detachment of amino group, methyl group and H_2O molecule from P8, followed by cleavage of the fourth ring and the carbonyl loss to produce P10 ($m/z = 349$) and P11 ($m/z = 275$). As a further degradation intermediates of P11, the P5 was also generated due to ring opening and hydroxylation reaction. For the pathway III, tetracycline molecule was fragmented into P12 ($m/z = 427$) through the dehydration reaction due to the tautomerization of keto-enol [47,65], then the fourth ring and its linked functional groups in P12 were eliminated to generate P13 ($m/z = 259$). P14 ($m/z = 209$) and P15 ($m/z = 153$) were subsequently obtained through the cleavage of the ring and hydroxylation. Finally, the small straight chain molecular structure of P16 ($m/z = 103$) was generated due to the break of benzene ring under the joint attack of reactive species [62], and a part of generated intermediates were decomposed into CO_2 and H_2O via further oxidation reaction.

The toxicities of intermediates were necessary to be considered for tetracycline degradation in H-VL-PEF system. As a popular broad-spectrum antibiotic, tetracycline can inhibit the growth of bacteria by the binding of the diethylamino group to the ribosomes during polypeptide elongation [66]. Therefore, the *Escherichia coli* growth inhibition experiments were carried out to estimate the toxicities of tetracycline solution and reaction samples by optical density and the diameter of the inhibition zone (Fig. 11). As shown in Fig. 11a, the *Escherichia coli* growth inhibition ratio slightly decreased from 89.0 ± 0.2% to 87.9 ± 0.4% after 10 min, indicating that some intermediates generated at the initial stage of the reaction remain a certain toxicity. However, the *Escherichia coli* growth was significantly inhibited with the prolonging of reaction time, and the inhibition ratio degreased from 83.9 ± 0.3% in 20 min to 65.4 ± 1.4% in 90 min. Additionally, the *Escherichia coli* inhibition zone diameter of tetracycline solution was 14.0 mm (Fig. 11b), whereas that of the sample after 90 min degradation decreased to 11.0 mm (Fig. 11c). The result of *Escherichia coli* growth inhibition experiments revealed that antimicrobial activities decreased to some extent after tetracycline was degraded in H-VL-PEF system.

According to the QSAR prediction, the acute toxicities of tetracycline and its intermediates in aquatic environments were further evaluated by the median lethal concentrations of Daphnia magna (LC_{50}-48 h), and fathead minnow (LC_{50}-96 h). Fig. 12a illustrated that the LC_{50}-48 h value of tetracycline was 8.7 mg L^{-1}, which was classified as "toxic" for Daphnia magna. Except for P1 (3.2 mg L^{-1}), P12 (1.9 mg L^{-1}) and P13 (8.4 mg L^{-1}), other intermediates exhibited higher LC_{50}-48 h values than tetracycline and became "harmful" for Daphnia magna result from their higher LC_{50}-48 h values than 10 mg L^{-1}. The LC_{50}-96 h values of intermediates had an increase in various degrees (from 0.9 mg L^{-1} of tetracycline to 3.1 – 396.1 mg L^{-1} of different intermediates), except

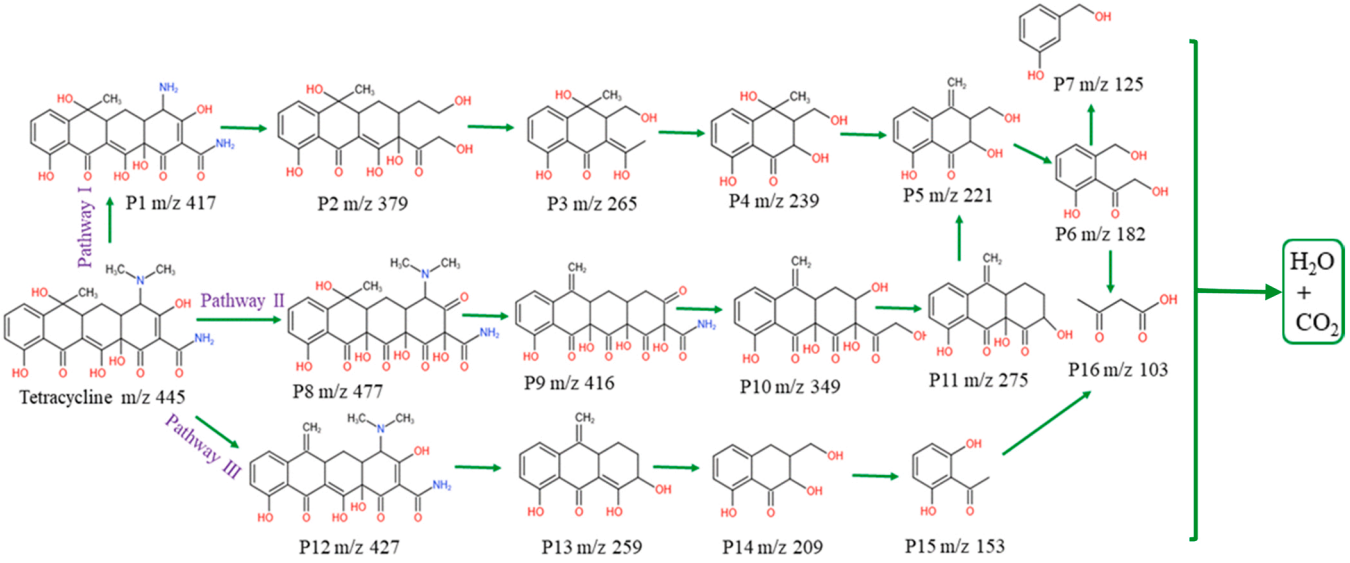

Fig. 10. Proposed degradation pathways of tetracycline in H-VL-PEF system.

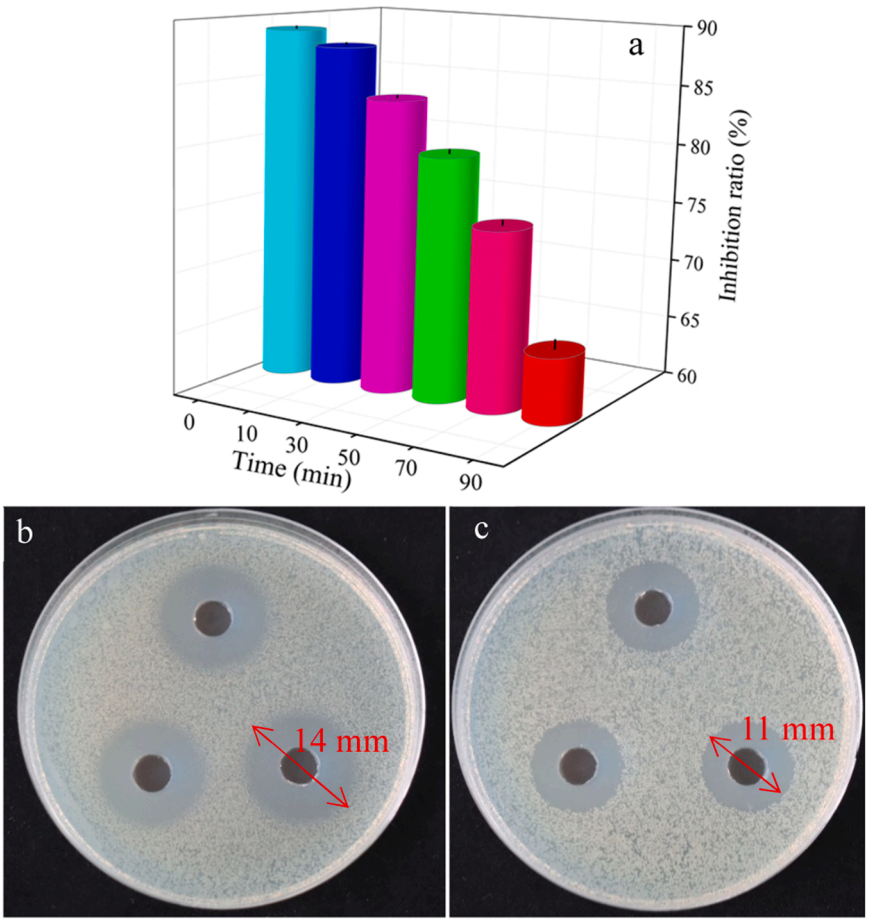

Fig. 11. *Escherichia coli* growth inhibition ratio of tetracycline solution and reaction samples (a), the *Escherichia coli* inhibition zone of tetracycline solution (b) and the sample after 90 min degradation (c).

that of P1, P12 and P13 reduced to 0.47, 0.29 and 0.69 mg L^{-1}, respectively (Fig. 12b). Although P1, P12 and P13 had high acute toxicity, the LC_{50}-48 h and LC_{50}-96 h values of further intermediates were dramatically higher than tetracycline, suggesting that H-VL-PEF system could reduce acute toxicity of tetracycline. Moreover, development toxicity and mutagenicity were used to predict the potential toxicities of tetracycline and its intermediates. As shown in Fig. 12c and d, tetracycline was "developmental toxicant" and "mutagenicity positive" due to that its developmental toxicity and mutagenicity were higher than 0.5, whereas three "developmental non-toxicant" (i.e., P4, P14 and P15) and six "mutagenicity positive" (i.e., P4, P6, P7, P12, P15 and P16) intermediates were identified after degradation. Although some intermediates still maintained toxicity, the comprehensive toxicity of tetracycline could be alleviated in H-VL-PEF system, and the TOC removal efficiency reached 93.8 ± 0.9% by prolonging the degradation time to 210 min (Fig. S16). Furthermore, H-VL-PEF system performed well performance for tetracycline degradation and TOC removal compared with previous H-EF or H-PEF systems and the results were record in Table 1. These results demonstrated that the H-VL-PEF system is an efficient and promising technique for tetracycline degradation.

4. Conclusions

The present work constructed a H-VL-PEF system with NO/PC-GDE as cathode and $CuFeO_2$/biochar as particle catalyst for tetracycline degradation under visible light. The NO/PC was prepared with alfalfa as a carbon precursor by pyrolysis method and possessed the H_2O_2 selectivity of 85.3% at − 0.423 V (vs. Ag/AgCl) according to RRDE result. The fabricated NO/PC-GDE could effectively generate H_2O_2 and exhibited high stability due to its surface good hydrophobicity. $CuFeO_2$/biochar was synthesized by hydrothermal method without extra reductant and showed a wide absorption under visible-light region. The tetracycline degradation efficiency was 97.7 ± 0.8% after 90 min reaction under optimal degradation conditions (100 mg L^{-1} $CuFeO_2$/biochar, 80 mA cm^{-2} of current density and pH 5.0) in H-VL-PEF system. The presence of Cl^- had almost no influence on tetracycline degradation, whereas the addition of NO_3^-, HCO_3^- and PO_4^{3-} significantly deteriorated tetracycline degradation. H-VL-PEF system had high stability due to that the tetracycline degradation efficiency only declined by 12.3% after 10 cycles. The $HO^•$ and electrons were the predominant reactive species, and $O_2^{•-}$ was subsidiary species for tetracycline degradation in H-VL-PEF system. The electrons generated on $CuFeO_2$/biochar by electrostatic induction and light excitation promoted the regeneration of $\equiv Cu^{2+}$-OH to $\equiv Cu^{+}$-OH and $\equiv Fe^{3+}$-OH to $\equiv Fe^{2+}$-OH, which was conducive to the production of active radicals. The degradation pathway of tetracycline was clarified through identifying major intermediates under HPLC/MS positive ion model. *Escherichia coli* growth inhibition experiments demonstrated that antimicrobial activities could be inhibited after tetracycline was degraded in H-VL-PEF system. The QSAR prediction of tetracycline and its intermediates confirmed that the acute and potential toxicities could be alleviated by prolonging the degradation time. The present results indicated the H-VL-PEF system is an efficient and promising strategy for tetracycline degradation.

CRediT authorship contribution statement

Shuaishuai Xin: Investigation, Formal analysis, Writing – original draft. **Siyue Huo**: Investigation, Formal analysis. **Chunlei Zhang:**

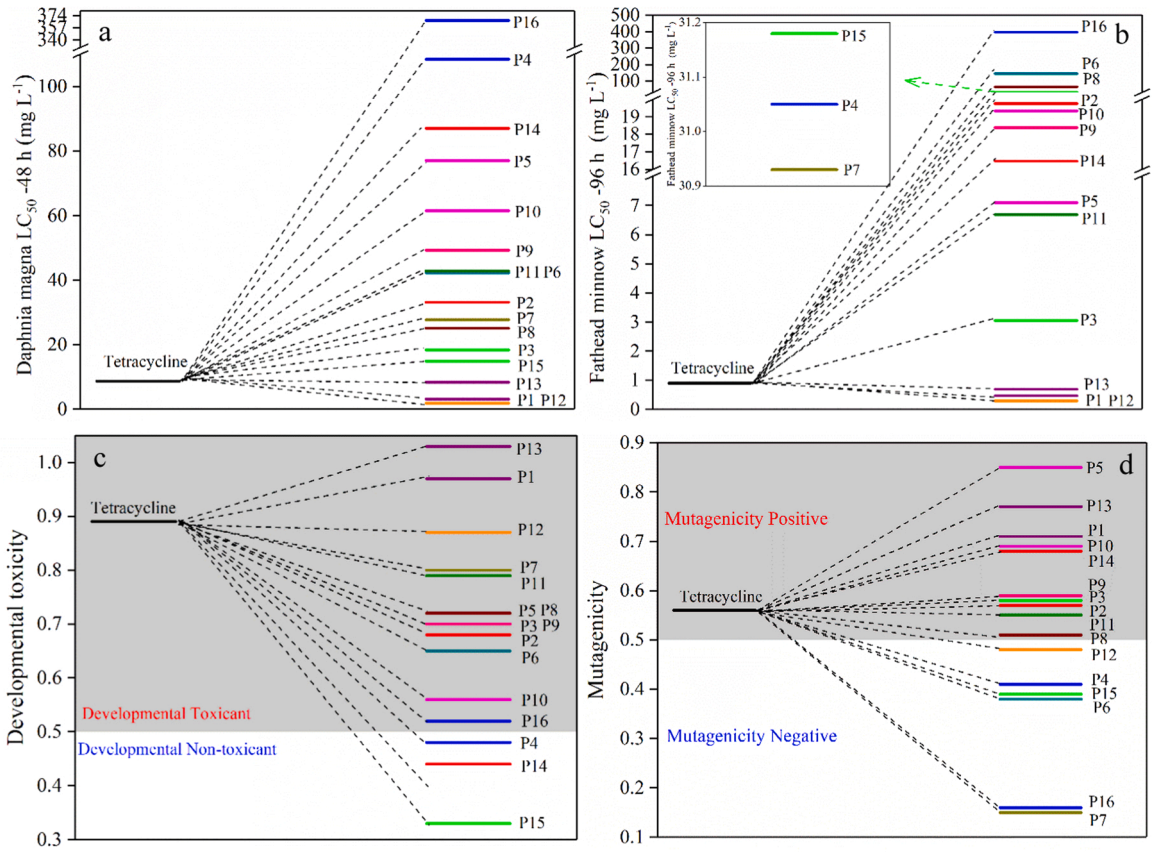

Fig. 12. Daphnia magna LC50–48 h (a), fathead minnow LC50–96 h (b), developmental toxicity (c) and mutagenicity (d) of tetracycline and its intermediates in H-VL-PEF system.

Table 1
Comparison of H-VL-PEF performance with previous systems.

Tetracycline concentration	Electrodes	Catalyst	Degradation efficiency	TOC removal	Refs
20 μg L^{-1}	Anode: Pt gauze Cathode: Fe_3O_4-graphite	Fe_3O_4	100% after 150 min	84.3% after 600 min	[67]
0.04 mM	Anode: Ti sheet Cathode: AuNCs/CNT filter	Gold nanoclusters	49.3% after 120 min	–	[68]
50 mg L^{-1}	Anode: Pt Cathode: Activated carbon filter	Fe@Fe_2O_3- CeO_2	90.7% after 60 min	86.9% after 360 min	[69]
20 mg L^{-1}	Anode: Pt Cathode: Activated carbon filter	Fe_2Co_1/PC	73.8% after 60 min	~80% after 240 min	[30]
20 mg L^{-1}	Anode: Ti/IrO_2-RuO_2 Cathode: CFF/CNT	Cu-doped Fe@Fe_2O_3	98.1% after 120 min	~90% after 480 min	[70]
20 mg L^{-1}	Anode: Pt Cathode: NO/PC-GDE	$CuFeO_2$/biochar	97.7% after 90 min	93.8% after 210 min	Present Study

Investigation. **Xiaoming Ma**: Investigation. **Wenjie Liu**: Investigation. **Yanjun Xin**: Supervision. **Mengchun Gao**: Conceptualization, Writing – review & editing, Supervision, Funding acquisition.

Declaration of Competing Interest

The authors declare that they have no known competing financial interests or personal relationships that could have appeared to influence the work reported in this paper.

Acknowledgments

The work was funded by the National Natural Science Foundation of China (No. 21878280).

Appendix A. Supporting information

Supplementary data associated with this article can be found in the online version at doi:10.1016/j.apcatb.2021.121024.

References

[1] X. Ao, W. Sun, S. Li, C. Yang, C. Li, Z. Lu, Degradation of tetracycline by medium pressure UV-activated peroxymonosulfate process: influencing factors, degradation pathways, and toxicity evaluation, Chem. Eng. J. 361 (2019) 1053–1062, https://doi.org/10.1016/j.cej.2018.12.133.

[2] X. Huang, N. Zhu, F. Mao, Y. Ding, S. Zhang, H. Liu, F. Li, P. Wu, Z. Dang, Y. Ke, Enhanced heterogeneous photo-Fenton catalytic degradation of tetracycline over yCeO2/Fh composites: performance, degradation pathways, Fe^{2+} regeneration and mechanism, Chem. Eng. J. 392 (2020), 123636, https://doi.org/10.1016/j.cej.2019.123636.

[3] R. Ocampo-Perez, J. Rivera-Utrilla, C. Gomez-Pacheco, M. Sanchez-Polo, J. Lopez-Penalver, Kinetic study of tetracycline adsorption on sludge-derived adsorbents in

aqueous phase, Chem. Eng. J. 213 (2012) 88–96, https://doi.org/10.1016/j.cej.2012.09.072.
[4] K. Yang, Q. Yue, J. Kong, P. Zhao, B. Gao, Microbial diversity in combined UAF-UBAF system with novel sludge and coal cinder ceramic fillers for tetracycline wastewater treatment, Chem. Eng. J. 285 (2016) 319–330, https://doi.org/10.1016/j.cej.2015.10.019.
[5] P. Wang, Y. He, C. Huang, Reactions of tetracycline antibiotics with chlorine dioxide and free chlorine, Water Res. 45 (2011) 1838–1846, https://doi.org/10.1016/j.watres.2010.11.039.
[6] M.H. Khan, H. Bae, J. Jung, Tetracycline degradation by ozonation in the aqueous phase: proposed degradation intermediates and pathway, J. Hazard. Mater. 181 (2010) 659–665, https://doi.org/10.1016/j.jhazmat.2010.05.063.
[7] N. Oturan, J. Wu, H. Zhang, V.K. Sharma, M.A. Oturan, Electrocatalytic destruction of the antibiotic tetracycline in aqueous medium by electrochemical advanced oxidation processes: effect of electrode materials, Appl. Catal. B Environ. 140–141 (2013) 92–97, https://doi.org/10.1016/j.apcatb.2013.03.035.
[8] M. El Kateb, C. Trellu, A. Darwich, M. Rivallin, M. Bechelany, S. Nagarajan, S. Lacour, N. Bellakhal, G. Lesage, M. Héran, M. Cretin, Electrochemical advanced oxidation processes using novel electrode materials for mineralization and biodegradability enhancement of nanofiltration concentrate of landfill leachates, Water Res. 162 (2019) 446–455, https://doi.org/10.1016/j.watres.2019.07.005.
[9] W. Yang, M. Zhou, N. Oturan, M. Bechelany, M. Cretin, M.A. Oturan, Highly efficient and stable FeIIFeIII LDH carbon felt cathode for removal of pharmaceutical ofloxacin at neutral pH, J. Hazard. Mater. 393 (2020), 122513, https://doi.org/10.1016/j.jhazmat.2020.122513.
[10] B.O. Orimolade, B.N. Zwane, B.A. Koiki, M. Rivallin, M. Bechelany, N. Mabuba, G. Lesage, M. Cretin, O.A. Arotiba, Coupling cathodic electro-fenton with anodic photo-electrochemical oxidation: a feasibility study on the mineralization of paracetamol, J. Environ. Chem. Eng. 8 (2020), 104394, https://doi.org/10.1016/j.jece.2020.104394.
[11] Y. Zhang, Z. Chen, P. Wu, Y. Duan, L. Zhou, Y. Lai, F. Wang, S. Li, Three-dimensional heterogeneous Electro-Fenton system with a novel catalytic particle electrode for bisphenol A removal, J. Hazard. Mater. 393 (2020), 120448, https://doi.org/10.1016/j.jhazmat.2019.03.067.
[12] Q. Chang, P. Zhang, A.H.B. Mostaghimi, X. Zhao, S.R. Denny, J.H. Lee, H. Gao, Y. Zhang, H.L. Xin, S. Siahrostami, J.G. Chen, Z. Chen, Promoting H_2O_2 production via 2-electron oxygen reduction by coordinating partially oxidized Pd with defect carbon, Nat. Commun. 11 (2020) 2178, https://doi.org/10.1038/s41467-020-15843-3.
[13] E. Jung, H. Shin, B.H. Lee, V. Efremov, T. Hyeon, Atomic-level tuning of Co-N-C catalyst for high-performance electrochemical H_2O_2 production, Nat. Mater. 19 (2020) 436–442, https://doi.org/10.1038/s41563-019-0571-5.
[14] K. Jiang, S. Back, A.J. Akey, C. Xia, H. Wang, Highly selective oxygen reduction to hydrogen peroxide on transition metal single atom coordination, Nat. Commun. 10 (2019) 3997, https://doi.org/10.1038/s41467-019-11992-2.
[15] L. Lai, J.R. Potts, D. Zhan, L. Wang, C.K. Poh, C. Tang, H. Gong, Z. Shen, J. Lin, R. S. Ruoff, Exploration of the active center structure of nitrogen-doped graphene-based catalysts for oxygen reduction reaction, Energy Environ. Sci. 5 (2012) 7936–7942, https://doi.org/10.1039/C2EE21802J.
[16] Z. Lu, G. Chen, S. Siahrostami, Z. Chen, Y. Cui, High-efficiency oxygen reduction to hydrogen peroxide catalysed by oxidized carbon materials, Nat. Catal. 1 (2018) 156–162, https://doi.org/10.1038/s41929-017-0017-x.
[17] B. Zhang, C. Wang, D. Liu, Y. Liu, X. Yu, L. Wang, Boosting ORR electrocatalytic performance of metal-free mesoporous biomass carbon by synergism of huge specific surface area and ultrahigh pyridinic nitrogen doping, ACS Sustain. Chem. Eng. 6 (2018) 13807–13812, https://doi.org/10.1021/acssuschemeng.8b01876.
[18] B. Jing, S. You, Y. Ma, Z. Xing, H. Chen, Y. Dai, C. Zhang, N. Ren, J. Zou, Fe_3Se_4/FeSe heterojunctions in cornstalk-derived N-doped carbon framework enhance charge transfer and cathodic oxygen reduction reaction to boost bio-electricity generation, Appl. Catal. B Environ. 244 (2019) 465–474, https://doi.org/10.1016/j.apcatb.2018.11.074.
[19] X. Wu, K. Chen, Z. Lin, Y. Zhang, H. Meng, Nitrogen doped graphitic carbon from biomass as non noble metal catalyst for oxygen reduction reaction, Mater. Today Energy 13 (2019) 100–108, https://doi.org/10.1016/j.mtener.2019.05.004.
[20] M.J. Kim, J.E. Park, S. Kim, M.S. Lim, A. Jin, O.H. Kim, M.J. Kim, K.S. Lee, J. Kim, S.S. Kim, Biomass-derived air cathode materials: pore-controlled S,N-Co-doped carbon for fuel cells and metal-air batteries, ACS Catal. 9 (2019) 3389–3398, https://doi.org/10.1021/acscatal.8b03730.
[21] Choi Yong-Keun, Kan Eunsung, Effects of pyrolysis temperature on the physicochemical properties of alfalfa-derived biochar for the adsorption of bisphenol A and sulfamethoxazole in water, Chemosphere 218 (2018) 741–748, https://doi.org/10.1016/j.chemosphere.2018.11.151.
[22] C. Zhao, S. Zhang, M. Han, X. Zhang, Y. Liu, W. Li, C. Chen, G. Wang, H. Zhang, H. Zhao, Ambient electrosynthesis of ammonia on a biomass-derived nitrogen-doped porous carbon electrocatalyst: contribution of pyridinic nitrogen, ACS Energ. Lett. 4 (2019) 377–383, https://doi.org/10.1021/acsenergylett.8b02138.
[23] S. Meng, Z. Mo, Z. Li, R. Guo, N. Liu, Oxygen-rich porous carbons derived from alfalfa flowers for high performance supercapacitors, Mater. Chem. Phys. 246 (2020), 122830, https://doi.org/10.1016/j.matchemphys.2020.122830.
[24] C. Li, C. Hu, Y. Song, Y.-M. Sun, W. Yang, M. Ma, Graphene-based synthetic fabric cathodes with specific active oxygen functional groups for efficient hydrogen peroxide generation and homogeneous electro-Fenton processes, Carbon 186 (2022) 699–710, https://doi.org/10.1016/j.carbon.2021.10.063.
[25] Y. Wang, M. Zhao, C. Hou, W. Chen, S. Li, R. Ren, Z. Li, Efficient degradation of perfluorooctanoic acid by solar photo-electro-Fenton like system fabricated by MOFs/carbon nanofibers composite membrane, Chem. Eng. J. 414 (2021), 128940, https://doi.org/10.1016/j.cej.2021.128940.
[26] G. Daniel, Y. Zhang, S. Lanzalaco, F. Brombin, C. Durante, Chitosan-derived nitrogen-doped carbon electrocatalyst for a sustainable upgrade of oxygen reduction to hydrogen peroxide in UV-assisted electro-Fenton water treatment, ACS Sustain. Chem. Eng. 38 (2020) 14425–14440, https://doi.org/10.1021/acssuschemeng.0c04294.
[27] L. Guo, F. Chen, X. Fan, W. Cai, J. Zhang, S-doped α-Fe_2O_3 as a highly active heterogeneous Fenton-like catalyst towards the degradation of acid orange 7 and phenol, Appl. Catal. B Environ. 96 (2010) 162–168, https://doi.org/10.1016/j.apcatb.2010.02.015.
[28] S. Huang, Q. Zhang, P. Liu, S. Ma, B. Xie, K. Yang, Y. Zhao, Novel up-conversion carbon quantum dots/α-FeOOH nanohybrids eliminate tetracycline and its related drug resistance in visible-light responsive Fenton system, Appl. Catal. B Environ. 263 (2020), 118336, https://doi.org/10.1016/j.apcatb.2019.118336.
[29] A.C.N. Pinheiro, T.S. Bernardino, F.E.B. Junior, M.R.V. Lanza, W.R.P. Barros, Enhanced electrodegradation of the sunset yellow dye in acid media by heterogeneous photoelectro-Fenton process using Fe_3O_4 nanoparticles as a catalyst, J. Environ. Chem. Eng. 8 (2020), 103621, https://doi.org/10.1016/j.jece.2019.103621.
[30] T. Hu, F. Deng, H. Feng, J. Zhang, B. Shao, C. Feng, W. Tang, L. Tang, Fe/Co bimetallic nanoparticles embedded in MOF-derived nitrogen-doped porous carbon rods as efficient heterogeneous electro-Fenton catalysts for degradation of organic pollutants, Appl. Mater. Today 24 (2021), 101161, https://doi.org/10.1016/j.apmt.2021.101161.
[31] N. Barhoumi, H. Olvera-Vargas, N. Oturan, D. Huguenot, A. Gadri, S. Ammar, E. Brillas, M.A. Oturan, Kinetics of oxidative degradation/mineralization pathways of the antibiotic tetracycline by the novel heterogeneous electro-Fenton process with solid catalyst chalcopyrite, Appl. Catal. B Environ. 209 (2017) 637–647, https://doi.org/10.1016/j.apcatb.2017.03.034.
[32] X. Jia, L. Xie, Z. Li, Y. Li, R. Ming, Q. Zhang, X. Mi, S. Zhan, Photo-electro-Fenton-like process for rapid ciprofloxacin removal: the indispensable role of polyvalent manganese in Fe-free system, Sci. Total Environ. 768 (2021), 144368, https://doi.org/10.1016/j.scitotenv.2020.144368.
[33] S. Xin, G. Liu, X. Ma, J. Gong, B. Ma, Q. Yan, Q. Chen, D. Ma, G. Zhang, M. Gao, Y. Xin, High efficiency heterogeneous Fenton-like catalyst biochar modified $CuFeO_2$ for the degradation of tetracycline: economical synthesis, catalytic performance and mechanism, Appl. Catal. B Environ. 280 (2021), 119386, https://doi.org/10.1016/j.apcatb.2020.119386.
[34] S. Xin, B. Ma, G. Liu, X. Ma, C. Zhang, X. Ma, M. Gao, Y. Xin, Enhanced heterogeneous photo-Fenton-like degradation of tetracycline over $CuFeO_2$/biochar catalyst through accelerating electron transfer under visible light, J. Environ. Manag. 285 (2021), 112093, https://doi.org/10.1016/j.jenvman.2021.112093.
[35] J. Qin, Q. Chen, C. Yang, Y. Huang, Research process on property and application of metal porous materials, J. Alloy. Compd. 654 (2016) 39–44, https://doi.org/10.1016/j.jallcom.2015.09.148.
[36] S.O. Ganiyu, M.J.G. de Araújo, E.C.T. de Araújo Costa, J.E.L. Santos, E.V. dos Santos, C.A. Martínez-Huitle, S.B.C. Pergher, Design of highly efficient porous carbon foam cathode for electro-Fenton degradation of antimicrobial sulfanilamide, Appl. Catal. B Environ. 283 (2021), 119652, https://doi.org/10.1016/j.apcatb.2020.119652.
[37] H. He, B. Jiang, J. Yuan, Y. Liu, X. Bi, S. Xin, Cost-effective electrogeneration of H_2O_2 utilizing HNO_3 modified graphite/polytetrafluoroethylene cathode with exterior hydrophobic film, J. Colloid Interface Sci. 533 (2019) 471–480, https://doi.org/10.1016/j.jcis.2018.08.092.
[38] I.N. Reddy, V. Manjunath, J. Shim, Structural and optical properties, electrochemical impedance spectroscopy, and Mott-Schottky analysis of $ZnFe_2O_4$ nanoparticle-decorated V_2O_5 rectangular nanosheets for photoelectrochemical applications, J. Environ. Chem. Eng. 9 (2021), 106131, https://doi.org/10.1016/j.jece.2021.106131.
[39] L. Li, C. Tang, Y. Zheng, B. Xia, S. Qiao, Tailoring selectivity of electrochemical hydrogen peroxide generation by tunable pyrrolic-nitrogen-carbon, Adv. Energy Mater. 10 (2020), 2000789, https://doi.org/10.1002/aenm.202000789.
[40] C. Lai, F. Huang, G. Zeng, D. Huang, L. Qin, M. Cheng, C. Zhang, B. Li, H. Yi, S. Liu, L. Li, L. Chen, Fabrication of novel magnetic $MnFe_2O_4$/bio-char composite and heterogeneous photo-Fenton degradation of tetracycline in near neutral pH, Chemosphere 224 (2019) 910–921, https://doi.org/10.1016/j.chemosphere.2019.02.193.
[41] J. Zhang, G. Zhang, S. Jin, Y. Zhou, J. Qu, Graphitic N in nitrogen-doped carbon promotes hydrogen peroxide synthesis from electrocatalytic oxygen reduction, Carbon 163 (2020) 154–161, https://doi.org/10.1016/j.carbon.2020.02.084.
[42] P. Su, M. Zhou, X. Lu, W. Yang, G. Ren, J. Cai, Electrochemical catalytic mechanism of N-doped graphene for enhanced H_2O_2 yield and in-situ degradation of organic pollutant, Appl. Catal. B Environ. 245 (2019) 583–595, https://doi.org/10.1016/j.apcatb.2018.12.075.
[43] S. Chen, Z. Chen, S. Siahrostami, T.R. Kim, D. Nordlund, D. Sokaras, S. Nowak, J. W.F. To, D. Higgins, R. Sinclair, J.K. Nørskov, T.F. Jaramillo, Z. Bao, Defective carbon-based materials for the electrochemical synthesis of hydrogen peroxide, ACS Sustain. Chem. Eng. 6 (2018) 311–317, https://doi.org/10.1021/acssuschemeng.7b02517.
[44] F. Hasché, M. Oezaslan, P. Strasser, T.-P. Fellinger, Electrocatalytic hydrogen peroxide formation on mesoporous non-metal nitrogen-doped carbon catalyst, J. Energ. Chem. 25 (2016) 251–257, https://doi.org/10.1016/j.jechem.2016.01.024.
[45] Q. Zhang, M. Zhou, G. Ren, Y. Li, X. Du, Highly efficient electrosynthesis of hydrogen peroxide on a superhydrophobic three-phase interface by natural air

diffusion, Nat. Commun. 11 (2020) 1731, https://doi.org/10.1038/s41467-020-15597-y.
[46] C. Wei, S. Sun, D. Mandler, X. Wang, S.Z. Qiao, Z.J. Xu, Approaches for measuring the surface areas of metal oxide electrocatalysts for determining their intrinsic electrocatalytic activity, Chem. Soc. Rev. 48 (2019) 2518, https://doi.org/10.1039/c8cs00848e.
[47] Y.Y. Chen, Y.L. Ma, J. Yang, L.Q. Wang, J.M. Lv, C.J. Ren, Aqueous tetracycline degradation by H_2O_2 alone: removal and transformation pathway, Chem. Eng. J. 307 (2017) 15–23, https://doi.org/10.1016/j.cej.2016.08.046.
[48] Q. Wu, H. Yang, L. Kang, Z. Gao, F. Ren, Fe-based metal-organic frameworks as Fenton-like catalysts for highly efficient degradation of tetracycline hydrochloride over a wide pH range: acceleration of Fe(II)/Fe(III) cycle under visible light irradiation, Appl. Catal. B Environ. 263 (2020), 118282, https://doi.org/10.1016/j.apcatb.2019.118282.
[49] M.R. Haider, W.L. Jiang, J.L. Han, H.M.A. Sharif, Y.C. Ding, H.Y. Cheng, A. J. Wang, In-situ electrode fabrication from polyaniline derived N-doped carbon nanofibers for metal-free electro-Fenton degradation of organic contaminants, Appl. Catal. B Environ. 256 (2019), 117774, https://doi.org/10.1016/j.apcatb.2019.117774.
[50] W. Zhou, X. Meng, J. Gao, F. Sun, G. Zhao, Janus graphite felt cathode dramatically enhance the H_2O_2 yield from O_2 electroreduction by the hydrophilicity-hydrophobicity regulation, Chemosphere 278 (2021), 130382, https://doi.org/10.1016/j.chemosphere.2021.130382.
[51] Y. Ding, H. Tang, X. Han, L. Zhu, W. Nan, Degradation of bisphenol A by hydrogen peroxide activated with $CuFeO_2$ microparticles as a heterogeneous Fenton-like catalyst: efficiency, stability and mechanism, Chem. Eng. J. 236 (2014) 251–262, https://doi.org/10.1016/j.cej.2013.09.051.
[52] F. Ghanbari, M. Riahi, B. Kakavandi, X. Hong, K.Y.A. Lin, Intensified peroxydisulfate/microparticles-zero valent iron process through aeration for degradation of organic pollutants: kinetic studies, mechanism and effect of anions, J. Water Process Eng. 36 (2020), 101321, https://doi.org/10.1016/j.jwpe.2020.101321.
[53] Y. Liu, X. He, Y. Fu, D.D. Dionysiou, Degradation kinetics and mechanism of oxytetracycline by hydroxyl radical-based advanced oxidation processes, Chem. Eng. J. 284 (2016) 1317–1327, https://doi.org/10.1016/j.cej.2015.09.034.
[54] P. Neta, R.E. Huie, Rate constants for reactions of nitrogen oxide (NO_3) radicals in aqueous solutions, J. Phys. Chem. B 90 (1986) 4644–4648, https://doi.org/10.1021/j100410a035.
[55] S. Xin, B. Ma, C. Zhang, X. Ma, P. Xu, G. Zhang, M. Gao, Y. Xin, Catalytic activation of peroxydisulfate by alfalfa-derived nitrogen self-doped porous carbon supported $CuFeO_2$ for nimesulide degradation: performance, mechanism and DFT calculation, Appl. Catal. B Environ. 294 (2021), 120247, https://doi.org/10.1016/j.apcatb.2021.120247.
[56] L. Lai, H. Ji, H. Zhang, R. Liu, B. Lai, Activation of peroxydisulfate by V-Fe concentrate ore for enhanced degradation of carbamazepine: surface ≡V(III) and ≡V(IV) as electron donors promoted the regeneration of ≡Fe(II), Appl. Catal. B Environ. 282 (2021), 119559, https://doi.org/10.1016/j.apcatb.2020.119559.
[57] N. Schmachtenberg, S. Silvestri, J. da Silveira Salla, G.L. Dotto, D. Hotza, S.L. Jahn, E.L. Foletto, Preparation of delafossite–type $CuFeO_2$ powders by conventional and microwave–assisted hydrothermal routes for use as photo-Fenton catalysts, J. Environ. Chem. Eng. 7 (2019), 102954, https://doi.org/10.1016/j.jece.2019.102954.
[58] M. Cheng, Y. Liu, D. Huang, C. Lai, G. Zeng, J. Huang, Z. Liu, C. Zhang, C. Zhou, L. Qin, W. Xiong, H. Yi, Y. Yang, Prussian blue analogue derived magnetic Cu-Fe oxide as a recyclable photo-Fenton catalyst for the efficient removal of sulfamethazine at near neutral pH values, Chem. Eng. J. 362 (2019) 865–876, https://doi.org/10.1016/j.cej.2019.01.101.
[59] A.A. Nada, B.O. Orimolade, H.H. El-Maghrabi, B.A. Koiki, M. Rivallin, M. F. Bekheet, R. Viter, D. Damberga, G. Lesage, I. Iatsunskyi, E. Coy, M. Cretin, O. A. Arotiba, M. Bechelany, Photoelectrocatalysis of paracetamol on Pd–ZnO/N-doped carbon nanofibers electrode, Appl. Mater. Today 24 (2021), 101129, https://doi.org/10.1016/j.apmt.2021.101129.
[60] X. Li, Y. Jia, J. Zhang, Y. Qin, Y. Wu, M. Zhou, J. Sun, Efficient removal of tetracycline by H_2O_2 activated with iron-doped biochar: performance, mechanism, and degradation pathways, Chin. Chem. Lett. (2021), https://doi.org/10.1016/j.cclet.2021.08.054.
[61] Z. Pi, X. Li, D. Wang, Q. Xu, Z. Tao, X. Huang, F. Yao, Y. Wu, L. He, Q. Yang, Persulfate activation by oxidation biochar supported magnetite particles for tetracycline removal: performance and degradation pathway, J. Clean. Prod. 235 (2019) 1103–1115, https://doi.org/10.1016/j.jclepro.2019.07.037.
[62] B. Zhang, X. He, X. Ma, Q. Chen, G. Liu, Y. Zhou, D. Ma, C. Cui, J. Ma, Y. Xin, In situ synthesis of ultrafine TiO_2 nanoparticles modified g-C_3N_4 heterojunction photocatalyst with enhanced photocatalytic activity, Sep. Purif. Technol. 247 (2020), 116932, https://doi.org/10.1016/j.seppur.2020.116932.
[63] G. Yang, Y. Liang, Z. Xiong, J. Yang, K. Wang, Z. Zeng, Molten salt-assisted synthesis of Ce_4O_7/Bi_4MoO_9 heterojunction photocatalysts for Photo-Fenton degradation of tetracycline: enhanced mechanism, degradation pathway and products toxicity assessment, Chem. Eng. J. 425 (2021), 130689, https://doi.org/10.1016/j.cej.2021.130689.
[64] A. Wang, Z. Zheng, H. Wang, Y.W. Chen, C.H. Luo, D. Liang, B. Hu, R. Qiu, K. Yan, 3D hierarchical H_2-reduced Mn-doped CeO_2 microflowers assembled from nanotubes as a high-performance Fenton-like photocatalyst for tetracycline antibiotics degradation, Appl. Catal. B Environ. 277 (2020), 119171, https://doi.org/10.1016/j.apcatb.2020.119171.
[65] J. Cao, L. Lai, B. Lai, G. Yao, X. Chen, L. Song, Degradation of tetracycline by peroxymonosulfate activated with zero-valent iron: performance, intermediates, toxicity and mechanism, Chem. Eng. J. 364 (2019) 45–56, https://doi.org/10.1016/j.cej.2019.01.113.
[66] J. Li, L. Zhao, R. Zhang, H.H. Teng, L.P. Padhye, P. Sun, Transformation of tetracycline antibiotics with goethite: mechanism, kinetic modeling and toxicity evaluation, Water Res. 199 (2021), 117196, https://doi.org/10.1016/j.watres.2021.117196.
[67] S. Liu, X.-r Zhao, H.-y Sun, R.-p Li, Y.-f Fang, Y.-p Huang, The degradation of tetracycline in a photo-electro-Fenton system, Chem. Eng. J. 231 (2013) 441–448, https://doi.org/10.1016/j.cej.2013.07.057.
[68] F. Liu, Y. Liu, Q. Yao, Y. Wang, X. Fang, C. Shen, F. Li, M. Huang, Z. Wang, W. Sand, J. Xie, Supported atomically-precise gold nanoclusters for enhanced flow-through electro-Fenton, Environ. Sci. Technol. 54 (2020) 5913–5921, https://doi.org/10.1021/acs.est.0c00427.
[69] J. Zhang, S. Qiu, H. Feng, T. Hu, Y. Wu, T. Luo, W. Tang, D. Wang, Efficient degradation of tetracycline using core–shell Fe@Fe_2O_3-CeO_2 composite as novel heterogeneous electro-Fenton catalyst, Chem. Eng. J. 428 (2022), 131403, https://doi.org/10.1016/j.cej.2021.131403.
[70] T. Luo, H. Feng, L. Tang, Y. Lu, W. Tang, S. Chen, J. Yu, Q. Xie, X. Ouyang, Z. Chen, Efficient degradation of tetracycline by heterogeneous electro-Fenton process using Cu-doped Fe@Fe_2O_3: mechanism and degradation pathway, Chem. Eng. J. 382 (2020), 122970, https://doi.org/10.1016/j.cej.2019.122970.